Journal of Asian Earth Sciences 221 (2021) 104946

Contents lists available at ScienceDirect

Journal of Asian Earth Sciences

journal homepage: www.elsevier.com/locate/jseaes

Elemental and C, O and Mg isotope geochemistry of middle-late Miocene carbonates from the Tuz Gölü Basin (Central Anatolia, Turkey): Evidence for Mediterranean incursions

Muazzez Çelik Karakaya *, Ayla Bozdağ, Necati Karakaya

Department of Geological Engineering, Faculty of Engineering and Natural Sciences, Konya Technical University, 42250 Selçuklu Konya, Turkey

ARTICLE INFO

Keywords:
Central anatolia
Dolomite
Evaporites
C, O and Mg isotopes
Magnesite
Tuz Gölü Basin

ABSTRACT

The Tuz Gölü basin, the largest of the Central Anatolian Neogene basins, is a NW-SE trending fault-controlled depression and includes many subbasins, such as the Ereğli, Ulukışla and Bor subbasins. In the basin, economically important evaporite deposits consisting mostly of halite, gypsum/anhydrite, glauberite and carbonates formed in the middle-late Miocene. The mineralogical and chemical properties and C, O and Mg isotopic compositions of the carbonate minerals that precipitated simultaneously with the other evaporite minerals were investigated using samples from boreholes to determine the precipitation conditions and paleoenvironment of the deposits.

The lack of covariance between the $\delta^{13}C$ and $\delta^{18}O$ values of the samples and the wide range of isotopic compositional variations indicate a basin that was hydrologically open to some degree. In addition, the lack of correlations between $\delta^{18}O$ values and MgO/(MgO + CaO), Mg/Ca and Sr/Ca ratios and the wide range of variations in both $\delta^{13}C$ and $\delta^{18}O$ values indicate that the carbonate minerals precipitated in a lagoonal environment where seawater incursions occurred through transgressions. The $\delta^{18}O$ values of the dolomite samples are higher than those of Messinian normal-salinity seawater dolomites and therefore require contributions from evaporative fluids. Additionally, the isotopic data indicate extreme fluctuations in temperature and the inflow-evaporation balance during carbonate precipitation and indicate that the evaporite minerals may have precipitated from the evaporation of seawater trapped within the basin during and after uplift of the region.

The Mg isotopic compositions of magnesium-rich carbonates are partially heterogeneous, and the $\delta^{26}Mg$ values are higher than the $\delta^{25}Mg$ values. Some of the $\delta^{26}Mg$ values are close to the $\delta^{26}Mg$ values of global seawater (–0.82‰) but higher than the global mean $\delta^{26}Mg$ value of river water (–1.09‰). The $\delta^{26}Mg$ values are partially within the range of marine sediments (–3.65 to +0.52‰), suggesting seawater contributions to carbonate precipitation.

1. Introduction

The study area is located in the southeastern part of the Tuz Gölü basin in the Central Anatolian Plateau (CAP) (Fig. 1). The CAP has undergone significant deformation since the late Miocene to Pliocene periods, and inner subbasins and many faults have been formed or reactivated (Dirik, 2001). The Tuz Gölü basin is bounded by nonparallel oblique-slip faults in the east-southeast and Central Taurus in the south (Kürçer and Gökten, 2014 and references therein). Additionally, the basin is one of the most important sedimentary basins of the CAP and is composed of many Neogene subbasins (Bala, Haymana, Ereğli, Ulukışla and Bor). Most of the basins in the CAP have been investigated by many researchers (Çemen et al., 1999; Dirik and Erol, 2000, 2003; Varol et al., 2002; Özsayın and Dirik, 2007; Tekin et al., 2007; Kürçer and Gökten, 2014; Fernández-Blanco et al., 2013; Özsayın et al., 2013; Gürbüz and Kazancı, 2014; Yavuz et al., 2017; Akgün et al., 2020; Meijers et al., 2020), and these researchers have reported that the surface sediments deposited in these basins are mostly fluvial or lacustrine. Gürbüz and Kazancı (2014) investigated the Miocene to Pliocene surface sediments in the Tuz Gölü basin and stated that the sediments were formed from terrestrial clastics and carbonates approximately 5000 m thick. Meijers et al. (2020) investigated the carbon and oxygen isotope compositions of

* Corresponding author.
E-mail address: mckarakaya@ktun.edu.tr (M.Ç. Karakaya).

https://doi.org/10.1016/j.jseaes.2021.104946
Received 7 March 2021; Received in revised form 3 September 2021; Accepted 4 September 2021
Available online 8 September 2021

outcropping carbonates in different parts of Central Anatolian including the study area, and indicated that the carbonates were formed under arid conditions and in a partially hydrologically closed lake basin during the late Miocene to Pliocene. However, the surface carbonates studied by Meijers et al. (2020) did not either interlayer or simultaneously precipitate with evaporite minerals such as halite, glauberite, thenardite, bloedite, magnesite, etc., and these evaporite minerals, are not also observed in surface. Therefore, the carbonates studied by Meijers et al. (2020) are not the same as carbonates taken from drillings subjected to the present study. Akgün et al. (2020) also studied the palynological properties of the late Eocene to late Miocene surface sediments comprising mainly of fluvio-lacustrine siliciclastics and carbonates of the Ereğli and Ulukışla basins. They stated that the paleoclimate changed from humid-subtropical to warm temperate during the early Miocene to late Miocene. Subsurface sediments were only investigated by Kadınkız et al. (2017), and they reported that the sediments were precipitated in a playa lake environment based mostly on lithological data.

Many researchers (Cosentino et al., 2012; Fernández-Blanco et al., 2013; Schildgen et al., 2014) declared that the Tuz Gölü Basin was affected by approximately 2 km of basement subsidence during the deposition of evaporitic sequences in the Paleocene and middle Miocene, and a second regional subsidence phase took place and sedimentation restarted, which reached nearly 3.5 km of thickness. During the middle Miocene period, the Mediterranean reached its highest level, and thus, the southern Tuz Gölü Basin was covered by seawater. Meanwhile, marine sediments precipitated in the Adana, Mut-Ermenek, and Beyşehir regions, located nearly 50–100 km south and southwest of the study area and the southern part of the CAP (Bassant et al., 2005; Koç et al., 2017 and references therein) (Fig. 1). Many researchers (Schildgen et al., 2012a; Schildgen et al., 2012b; Cipollari et al., 2013; McNab et al., 2018) have pointed out that these marine sediments clearly indicate that a middle to late Miocene transgression phase reached to approximately 100 km into the interior part of the Anatolian from the Mediterranean coastline. Therefore, the transgression phase caused a sea level rise and incursion of seawater into the southernmost part of the Tuz Gölü Basin. Ćorić et al. (2012) identified Serravallian age mollusks within sandy-clay shallow marine sediments in the high plains north of the Mut basin. Around the Ermenek region, late Miocene marine sediments were deposited at 8 Ma at the onset of uplift (Cosentino et al., 2012). Karakaya et al. (2019) documented a diatom, *Dimidiata saccula*, which is of Sarmatian age (11.6 to 12.7 Ma) and characterizes the marine environment in the southern Tuz Gölü basin. In the study area, that seawater contribution was an important process in the precipitation of the middle Miocene evaporite minerals, as determined by the fluid inclusion (Karakaya et al., 2019) and stable isotope (B, Br, Cl, and Li) studies (Ercan et al., 2019) in halites. Additionally, Karakaya et al. (2020) investigated $\delta^{34}S$ and $\delta^{18}O$ values and $^{87}Sr/^{86}Sr$ ratios and explained that Ca-sulphates, collected from the boreholes precipitated mostly from Miocene seawater.

In the abovementioned studies, only middle and late Miocene surface deposits were investigated, but these sediments do not contain marine-originated indicative evaporite minerals such as halite, glauberite, magnesite, etc. which are a few 100 m thick and precipitate simultaneously with dolomite. In the present study, the investigated evaporite deposits are covered by Pliocene and Quaternary sediments with thickness of approximately 200–300 m. There has been no research done especially on the detailed mineralogical, chemical and some isotope compositions of the Miocene evaporites from subsurface sediments in the Tuz Gölü basin, except Ercan et al. (2019) and Karakaya et al. (2019, 2020).

Some evaporite deposits formed under the influence of the Messinian Salinity Crisis (MSC) have been reported in coastal sediments in southern Turkey (Adana, Hatay, İskenderun, Antalya) (Tekin et al., 2010; Ilgar et al., 2013; Aksu et al., 2018; Güneş et al., 2018). A connection can be hypothesized regarding the proximity of the known marine outcrops

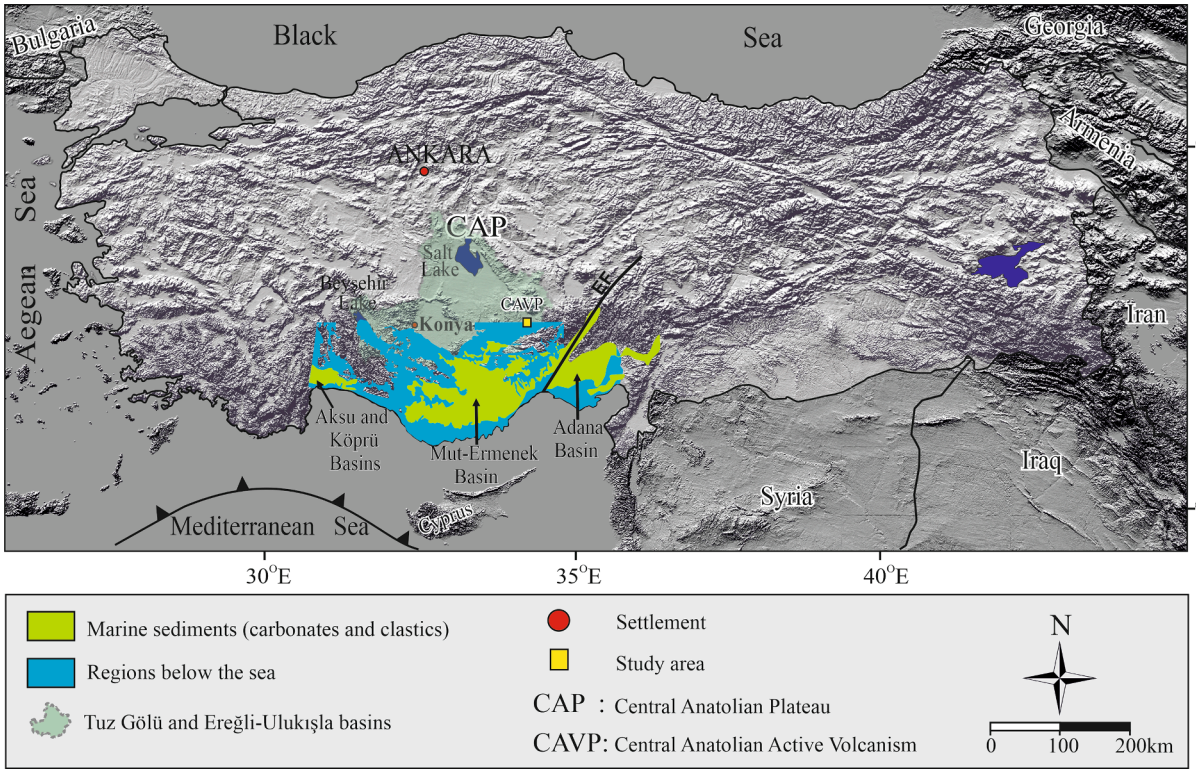

Fig. 1. Study area and paleogeographic map before 8 Ma on the current topographic map of Turkey. Blue regions indicating regions of modern topography that were below sea level prior to 7 to 8 Ma, and green regions show marine sediments (green and blue regions modified by Şafak et al., 2005; Schildgen et al., 2012b). (For interpretation of the references to color in this figure legend, the reader is referred to the web version of this article.)

and evaporitic facies between the MSC deposits in southern Turkey and the investigated evaporite deposits in the present study. Therefore, considering that the carbonate and evaporite deposits are closely related and precipitated in the same environment, in this study, we aimed to a) evaluate the factors that controlled the formation of minerals in the basin; b) reveal that the deposits were not precipitated in a completely inner basin; and c) interpret the paleoenvironment by using the mineralogical and chemical data (Mg, C and O isotopes). Thus, the mixing of sea water into the basin determined by the authors based on previous studies of halite and sulfates will be confirmed by the C, O and Mg isotope contents in carbonates, indicating that these rocks were not precipitated in continental basin.

2. Geological setting

In the study area, lithological units that are vertically and laterally transitional with each other were defined and named by Oktay (1982) as the Kızılbayır, Katrandedetepe, and Beştepeler Formations from bottom to top (Figs. 2, 3). However, the outcropping lithologies of the units in the study area are mainly composed of carbonates and clastics that are stratigraphically discontinuous and have laterally variable thicknesses. In the present study, the main lithological and mineralogical properties of the formations in the study area were defined from many boreholes. The Kızılbayır Formation consists of red to dark red colored sandstone, gray conglomerate and mudstones and is overlain by the Katrandedetepe and Beştepeler Formations.

The Katrandedetepe Formation is composed mostly of halite, (Ca-Na)- and Ca-sulfate, rarely Na-, NaMg-, and Mg-sulfate, and CaMg- and Mg-carbonate deposits (Figs. 3, 4). In particular, halite and glauberite (NaCa-sulfate) minerals have formed economically important reserves. The lower and middle levels of the formation consist mostly of halite-anhydrite/gypsum-glauberite-dolomite alternations and partly of magnesite, claystone, and bituminous shale, while the upper levels are composed mostly of limestone, mudstone, siltstone, and sandstone and partly of conglomerate and tuff/ignimbrite. The carbonate, evaporite and clay-marl beds/laminates generally show cm-scale cycles (Figs. 3, 5). The evaporite sequence shows synsedimentary and early diagenetic structures, including laminations, cross-bedding, and rarely ripple marks, micro-folds or slumps. Although the laminae are generally parallel, they are sometimes distorted based on the shapes of the upper and lower units and have developed a network structure that fills the gaps. Slump structures, nearly vertically inclined laminas, crushing and crack fillings have formed as a result of deformation. The deformation structures indicate subsidence or tectonic movements in the basin, while parallel lamination exhibits stagnation of environmental conditions during precipitation. These structures indicate an evaporitic environment that is closely associated with sabkhas (Warren, 2016). The evaporitic levels of the formation do not crop out and are covered by alluvial sediments with a thickness of approximately 250 m (Figs. 3, 4).

The Beştepeler Formation is represented by green-burgundy mudstone, sandstone, light green-gray colored gypsum, anhydrite and grain-supported sandstones and cream-colored lapilli tuff. Aydar et al. (2012) determined an age of 6.34 ± 0.07 Ma using Ar/Ar dating of the tuff. According to K/Ar dating, the age of the oldest tuffs in the study area was determined to be 8.96 Ma (Schumacher et al., 1990). According to these radiometric ages, the age of the Katrandedetepe Formation must be Upper Miocene (Tortonian - Messinian).

The carbonates are mainly limestone, clayey limestone, dolomite and clayey dolomite. The carbonate beds are mainly beige, white, or gray massive microcrystalline structures and exhibit laminated organic matter containing mudstones/black shales displaying a micritic texture. Dolomite is more common at moderate depths (400–500 m) in the drillings, while magnesite is less common and occurs from moderate to mostly deeper depths as massive/pure magnesite bands several cm thick. Carbonate-enriched layers are white to beige or gray in color (Fig. 5). The carbonate-enriched layers are sometimes crystallized around other minerals depending on the composition of the solution, tectonic events, and other diagenetic processes (e.g., burial temperature and pressure) in the basin. The determined carbonate minerals are mainly dolomite, partially magnesite, and rarely calcite, and the minerals are mostly observed as cement between the other evaporite minerals and sometimes as carbonate-enriched beds varying from several mm to several dm (Figs. 5, 6).

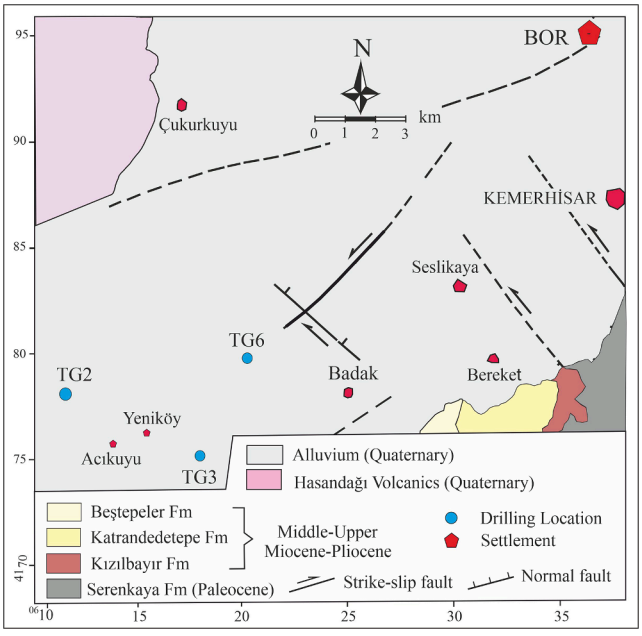

Fig. 2. Geological map of the study area and locations of the cores in the basin (revised from Oktay, 1982).

3. Methods

A total of 92 dolomite- and magnesite-containing samples taken from the Katrandedetepe Formation at different depths in three wells drilled by the MTA (General Directorate of Mineral Research and Exploration of Turkey) were investigated (Fig. 2). The mineralogical composition of the powdered samples (total fraction) was determined using X-ray diffraction (XRD) (Rigaku D/MAX 2200 PC, Japan, CuKα radiation, 40 kV and 40 mA and a scanning speed of 2°/min from 2 to 70° 2θ) at Hacettepe University (Ankara, Turkey). The semiquantitative mineral content was determined from powder XRD patterns according to the external standard method developed by Gündoğdu (1982) (Table 1). The accuracy of the method is reported by the author to be less than ±5%. After mineralogical analyses, the main and trace element contents of pure or dolomite/magnesite-rich core samples taken from drilling samples were determined using ICP-MS (Perkin-Elmer, Elan 6100 and ICP-MS: PN-EN ISO 17294-2:2006) in the ACME Laboratories (Canada) and AGH Laboratories (AGH University of Science and Technology in Krakow, Poland). The micromorphological properties of the carbonate minerals were investigated to determine their interrelations with other minerals and to examine their features using scanning electron microscopy (SEM, LEO 1430VP (Zeiss Cambridge, UK at Afyonkarahisar Kocatepe University)). The elemental contents of the minerals were determined by energy-dispersive X-ray spectroscopy (EDS) using an accelerating voltage of 15–20 kV, with a beam current of 15 mA and spot size of 5 mm. Samples were placed in a sample holder, dried at 50 °C for one hour and then coated with 5 μm of gold before SEM analysis.

The C and O isotopic compositions of dolomite/magnesite-enriched bulk samples taken from drillings of TG2 (4 samples), TG3 (10 samples) and TG6 (6 samples) were determined at the Environmental Isotope Laboratory, University of Waterloo, Canada. Carbon (^{13}C) and

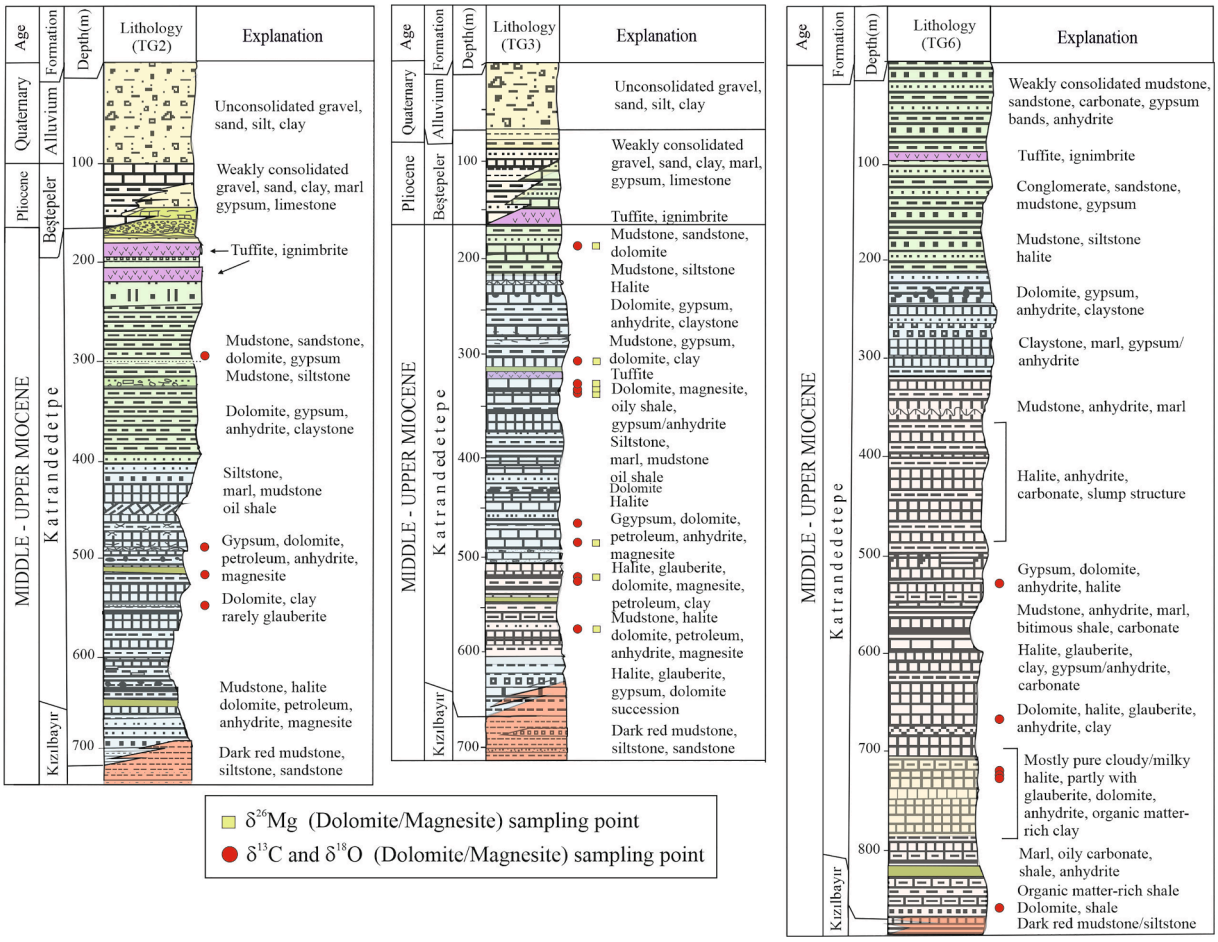

Fig. 3. Lithological and stratigraphic properties of the cores and dolomite- and magnesite-containing sampling points where $\delta^{13}C$ and $\delta^{18}O$ $\delta^{26}Mg$ analyses were performed.

oxygen (^{18}O) proportions were determined (better than ±0.2‰ vs. VPBD) by the production of carbon dioxide (CO_2) from carbonate minerals by reactions with 100% phosphoric acid (H_3PO_4) at 90 °C using standard procedures based on the methods of Epstein et al. (1953). Samples and standards were weighed into Exetainer™ septum vials and sealed and flushed with pure helium. Then, 100% phosphoric acid was injected into the vials, which were then placed in an aluminum tray that was kept at 90 ± 0.1 °C for>1 h. The CO_2 was extracted automatically with a double-hole needle Gilson autosampler connected to a GVI MultiFlow device. The MultiFlow contained a 500-µl sample loop and GC column that separated CO_2, N_2, O_2 and H_2O. Helium carrier gas then transported the purified CO_2 into a GVI IsoPrime continuous flow isotope ratio mass spectrometer system (CF-IRMs) that measured the isotope ratios. Four calibrated standards, EIL-21 (traceable to NBS-18 and NBS-19), IAEA-CO-1, IAEA-CO-8 and IAEA-CO-9, were used for normalization. Additional/alternate standards of the same composition as the samples were included. During a sample run, linearity checks were included using a suite of EIL-21 samples to produce a range of peak heights that encompass the expected sample peak range.

Mg isotope analyses and chemical separations were performed using a Thermo Scientific Neptune Plus multicollector-inductively coupled plasma-mass spectrometer (MC-ICP-MS) at the ALS laboratory (Sweden) following the procedure described by Wombacher et al. (2009) with control of analysis recoveries for each individual sample. Mg isotope compositions were referenced to the DSM3 isotope standard. The samples were prepared by a combination of HNO_3 + HF digestion and alkali fusion. Mg was separated from the sample matrix using ion-exchange, and Mg isotope reference materials (IRMs) were measured in purified fractions using a combination of internal standardization (Si isotopes) and external calibration with bracketing isotope standard reference materials (SRMs). Internal precision (from two measurements of the same Mg that were separated within the same measurement session) was in the range 0.06–0.08‰. The reproducibility of the entire procedure (from replicate separation/analysis of one sample) was better than 0.03‰. The external precision from n > 80 measurements of an in-house QC sample was 0.06‰. The method was originally validated using a set of certified reference materials (CRMs) (e.g., JB-2, JCp-1, CASS-4 and IRMM-3704) with agreement between the obtained and published Mg deltas of better than 0.1‰ (measure of accuracy). Standard deviations were calculated from two consecutive independent measurements.

4. Results

4.1. Mineralogical properties and facies types

Macroscopically magnesite exhibits a beige color and is in the form of laminates, while microscopically, it takes the form of crystals, or filling or cement in spaces between other evaporite minerals (Figs. 5, 6a, b). Bidirectional cleavage of coarse magnesite crystals is typically observed, and also prismatic, twin-shaped, or amorphous anhydrite residues are present within the mineral (Fig. 6a, c). The typical morphology of magnesite indicates that it formed by precipitation processes. Dolomite shows rhombic cleavage and micritic or microsparitic filling, but it was not observed as cement (Fig. 6d). In addition to secondary anhydrides, primary anhydrides without gypsum residues were also observed. Additionally, microcrystalline and partially euhedral

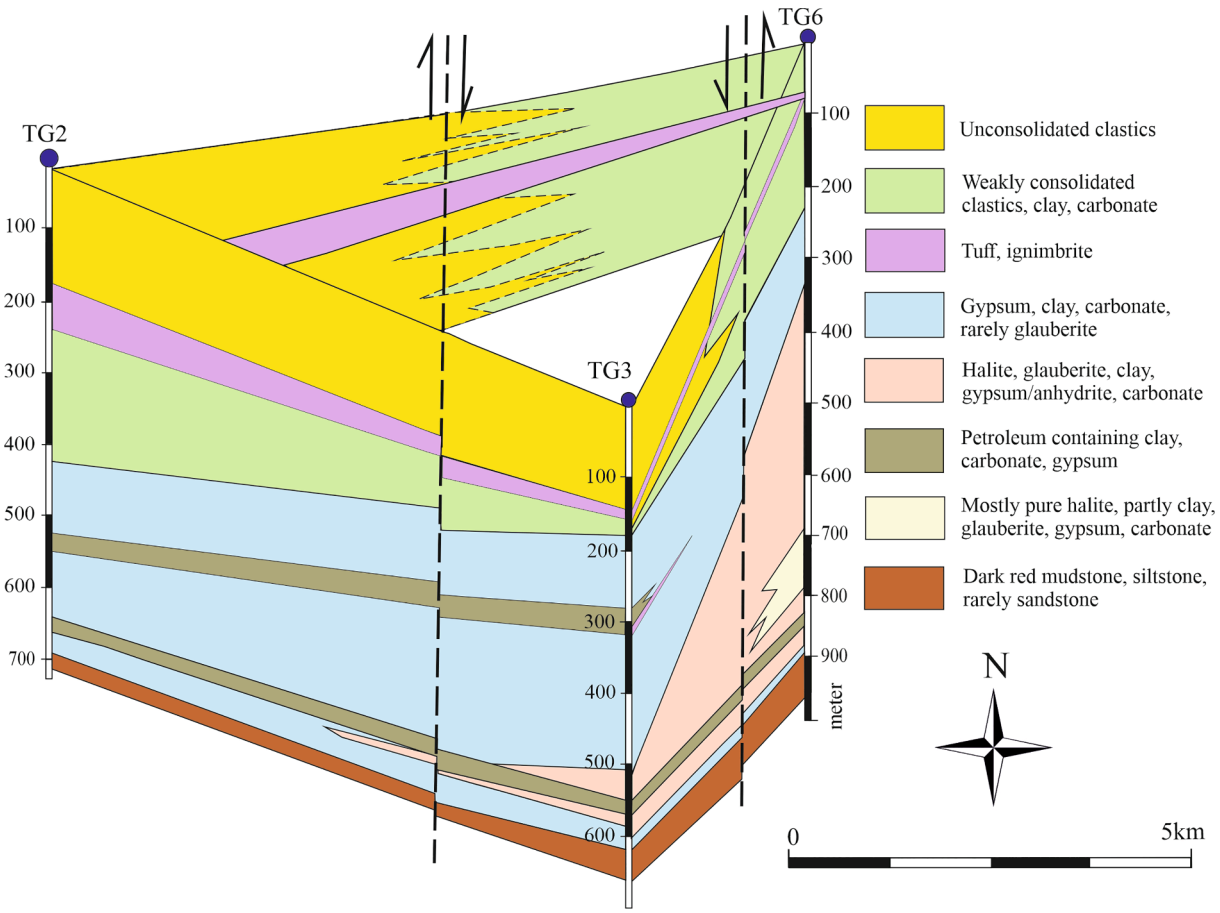

Fig. 4. Lithology of the boreholes and the lateral relationships among them.

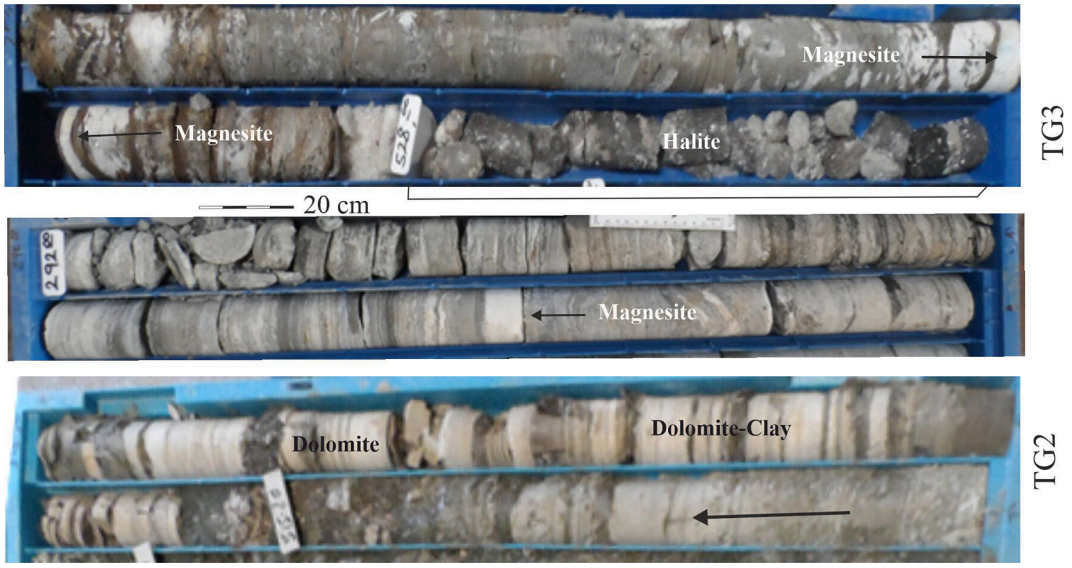

Fig. 5. Some core photos showing the main lithologies in the basin. Micritic dolomite and magnesites show alternations both upward and downward with anhydrite, glauberite, halite, clayey dolomite and organic matter-rich clayey marl (note: the arrow indicates the aspects of the boreholes).

crystals of magnesite and dolomite with Mg-rich smectite were detected (Fig. 7a, b). Some silicate minerals were observed as mainly detrital clastics (e.g., feldspar, quartz, and mica) and clay minerals (e.g., sepiolite, and Na/Mg-smectite) precipitated in the basin. The minerals are partially associated with glauberite, dolomite and magnesite in some layers or interlayered with evaporites. The clay minerals observed in evaporites, especially together with carbonates, indicate that there was a chemical precipitation in the basin and that the environment was stagnant.

Considering the mineralogical and textural features, various facies were defined and their properties and formation conditions can be explained as follows:

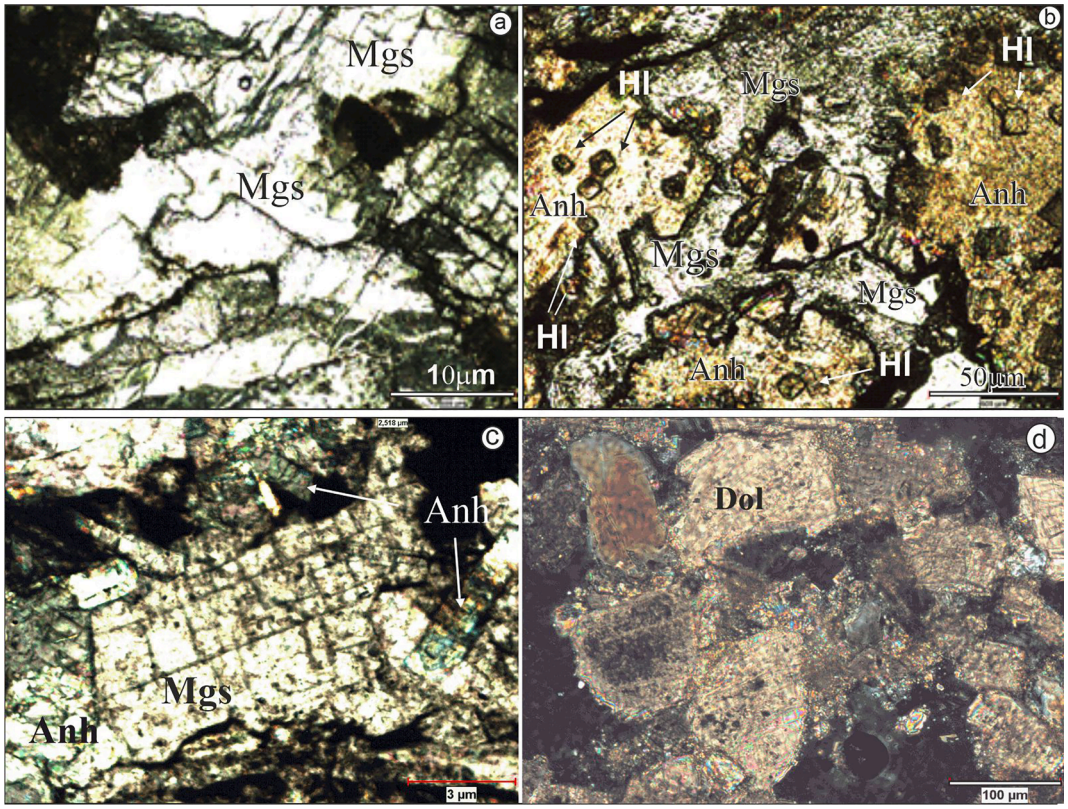

Fig. 6. Microscope photos of some samples under plane-polarized light: a, b) Crystal-form or filling intergranular spaces magnesite and anhydrite including microcrystalline hopper halite crystal with chevron structures (TG3 291.5, TG6 332 m, respectively). c) Magnesite showing typical cleavage planes and including anhydrite pseudomorphs (TG7 557 m). d) Micritic-microsparitic dolomite showing typical cleavage planes (TG6 693.6 m).

Table 1
$\delta^{18}O_{VPDB}$ and $\delta^{13}C_{VPDB}$ values (‰) and some elemental contents and ratios of dolomite and magnesite containing samples from different drillings in the basin.

Drill, Depth	Main Carbonate Mineral	$\delta^{13}C_{VPDB}$	$\delta^{18}O_{VPDB}$	A	Sr ppm	MgO %	CaO %	Mg/Ca	Sr/Ca mmol/mol
TG2 299.9	Dolomite	−9.2	2.4	0.55	310	21.05	24.24	0.73	0.08
TG2 497.7	Dolomite	−6.5	1.6	0.50	3203	19.13	26.34	0.61	0.78
TG2 515.5	Dolomite	−7.0	1.1	0.51	178	16.59	21.87	0.64	0.05
TG2 547.7	Dolomite	−9.8	−3.4	0.50	3168	18.31	25.55	0.60	0.79
TG3 177.3	Dolomite	−5.2	−1.5	0.53	401	15.15	18.85	0.68	0.14
TG3 315.1	Dolomite	−1.5	5.2	0.72	1115	17.51	9.62	1.54	0.74
TG3 330.15	Dolomite	−2.7	1.9	0.60	227	16.65	15.41	0.91	0.09
TG3 335.5	Dolomite	−2.4	1.2	0.49	273	13.42	19.40	0.58	0.09
TG3 341.9	Dolomite	−2.6	2.5	0.63	256	15.14	12.14	1.05	0.11
TG3 468.8	Dolomite	−10.8	0.9	0.46	923	22.04	36.70	0.51	0.16
TG3 489.3	Magnesite	−9.3	2.3	0.98	1314	41.74	1.29	27.30	5.79
TG3 528.4	Magnesite	−6.7	8.1	0.96	2285	35.98	2.21	13.74	6.62
TG3 529.2	Dolomite	−9.5	8.8	0.48	683	6.23	9.43	0.56	0.46
TG3 577.8	Dolomite	0.0	−3.0	0.27	1119	9.27	34.02	0.23	0.20
TG6 532.6	Dolomite	−5.3	1.2	0.26	2530	6.40	25.91	0.21	0.62
TG6 674.7	Magnesite	−4.8	7.6	0.72	3038	18.47	10.19	1.53	1.91
TG6 711.0	Magnesite	−5.1	10.5	0.62	832	11.19	9.39	1.01	0.57
TG6 717.2	Dolomite	−8.6	5.7	0.57	2098	13.58	14.32	0.80	0.94
TG6 718.2	Dolomite	−5.4	5.7	0.31	5346	8.10	25.54	0.27	1.34
TG6 874.0	Dolomite	−2.8	0.6	0.37	571	10.11	24.18	0.35	0.15

Note: A: MgO/(MgO + CaO).

Oolitic limestone lithofacies observed over clastic facies are composed of cream-gray colored medium-thick bedded oolitic limestone, fossiliferous oolitic limestone and oolitic limestone, and its thickness varies between 15 and 85 cm. Intact and fragmented bivalvia, ostracod and gastropod shell fossils, shell fragments of these fossils were observed. This facies characterizes a very shallow and turbulent environment in lakes, lagoons and coastal shallows as well as in subtidal environments (Tucker, 1991; Flügel, 2004) and very shallow basin conditions where the water level rises relatively. The clastics of this lithofacies may be exogenic or may have formed as a result of turbulence in the environment.

Gypsum-anhydrite-mudstone-micritic limestone facies forms mainly from gypsum-anhydrite and mudstone-micritic limestone lithofacies, and the facies generally has gray-light yellow and cream-colored lamina and thin and medium bedding. The average thickness of the facies varies from 250 to 300 m and its characteristic sedimentary structures are generally slip folds, salt diapiric structures, laminations, and cage structures. The lithological alternation indicates the frequency of water

Table 2
$\delta^{25}Mg$ and $\delta^{26}Mg$ values (‰) and Mg contents of samples containing dolomite and magnesite from the TG3 drilling.[1]

Sample ID (m), Mineral type and content (%)	Mg %	$\delta^{25}Mg$	SD	$\delta^{26}Mg$	SD
TG3-177.3 Dol(45) + Sme(34) + Anh(11.5) + Qz(6.5) + Fsp (3)	9.85	−0.323	0.064	−0.587	0.077
TG3-315.1 Dol(64) + Hl(17) + Gp(13) + Qz(6)	15.66	0.241	0.060	0.468	0.074
TG3-330.15 Dol(66) + Gp(21) + Hl(10) + Kln(3)	16.10	0.209	0.061	0.397	0.069
TG3-335.5 Dol(42) + Qz(31) + Gp(14) + Anh(8) + Hl(5)	8.90	−0.300	0.072	−0.617	0.075
TG3-341.9 Dol(46) + Fsp(21) + Gp(15) + Qz(11) + Hl(2)	9.85	0.026	0.059	0.052	0.071
TG3-489.3 Mgs(93) + Qz(4) + Sme(3)	23.17	0.175	0.064	0.355	0.070
TG3-528.4 Mgs(91) + Hl(5) + Sme(4)	21.70	−0.049	0.075	−0.074	0.079
TG3-577.8 Anh(79) + Dol(21)	25.89	0.457	0.061	0.882	0.063
TG3-577.8repeated	25.89	0.445	0.060	0.885	0.064
QCS (standard)		−1.911	0.088	−3.752	0.097

SD: standard deviation.
[1] Abbreviations: Anh: anhydrite, Dol: dolomite, Fsp: feldspar, Gp: gypsum, Hl: Halite, Kln: kaolinite, Qz: quartz, Mgs: magnesite, Sme: smectite.

entry into the basin and the change in the geochemical characteristics of the water. The frequency of water entry into the basin is related to seasonal changes or transgression and the fluctuation in the water. Water inflow mostly causes to the changes in the water composition and water level in the basin/environment. The carbonates, especially dolomite intercalated with other evaporite minerals, indicate that the amount of water in the basin was increased and that the basin water was diluted. Furthermore, the presence of anhydrite fillings in the shells of gastropods in the carbonates is an indication of the rapidity of precipitation and evaporation. Clastic sediments, which are frequently observed together with gypsum and have a normal gradation, may confirm that the basin was strongly recharged by transgression. After the deposition of the carbonate and gypsum/anhydrite lithofacies, halite-mudstone lithofacies, generally observed as only halite with a thickness of 4–5 m, alternated with glauberite or glauberite-rich halite or mudstones. The thickness of the facies in the medium and bottom levels of the drilling varies between a few cm and 50 m, but the facies is not observed toward the upper levels. Halite is observed in the form of very thick layers and between carbonate (mostly dolomite, rarely magnesite) and gypsum/anhydrite deposits in the sequence. It is not only in the form of pure halite but also generally intercalated with mudstones in the succession, indicating that the basin was constantly fed. The water depth of the basin changed over time, and the presence of the evaporites indicates to an arid climate. Additionally, the lithological sequence shows that the water level in the basin changed frequently, intense surface erosion developed, and arid-semiarid climatic conditions dominated.

Oily bituminous shale facies are composed of black mudstones that are highly dispersed, and show good fissility, and are peaty in places. In some parts, a very intense petroleum smell and viscous oil flow were observed. The thickness of the facies observed at levels close to the base of the Katrandedetepe Formation varies between 1.5 and 2 m. Rare peat formations were also observed in the facies rich in organic matter. This lithofacies reflects swamp environments rich in organic material during very shallow stagnant periods of the basin (lagoon). Additionally, the abundance of mudstones indicates that the ambient conditions are quite calm (Tucker, 1991).

4.2. Elemental and isotopic composition

The MgO/(MgO + CaO) ratio of the dolomite-rich samples ranges from 0.26 to 0.72, while the ratio of the magnesite-rich samples varies between 0.62 and 0.98. The Sr/Ca ratios of the dolomite-rich samples range from 0.08 to 1.34, while the ratios of the magnesite-rich samples vary between 0.57 and 6.62. The Sr and MgO contents of the samples containing carbonate minerals fluctuate between 178 and 5346 ppm and 6.23 and 41.74%, respectively. Considering all samples from the TG3 drilling, very high Sr contents (as high as 15614 ppm) were also observed. The Li, B, Br and Sr contents of especially samples taken from between 157 and 330 m in the drilling are higher than those of in the lower levels (Fig. 8, Table 3), and none of these elements are correlated with Ca or Mg. The boron contents in the TG3 drilling samples range from 11 to 1453 ppm, and the lithium contents vary between 1 and 316 ppm. The Br content of all samples varies from 11 to1774 ppm, while the Br content of the carbonate-enriched samples ranges between 40 and 472 ppm (Tables 1–3).

The $\delta^{18}O$ values of dolomite samples from the TG2 drilling range from −3.38 to 2.37‰, while the $\delta^{13}C$ isotope values range from −9.81 to −6.5‰. The $\delta^{18}O$ and $\delta^{13}C$ values of the two magnesite-rich samples from the TG3 drilling range from 7.6 to 10.5‰ and from −4.8 to −5.1‰, respectively (Table 1). The $\delta^{18}O$ values of the dolomite samples from the TG3 drilling range from −3.0 to 5.2‰, and the $\delta^{13}C$ isotope values range from −10.8 to 0.04‰ (Table 1, Fig. 8). The $\delta^{18}O$ and $\delta^{13}C$ isotope values of the dolomite samples from the TG6 drilling range from 0. 6 to 5.7‰ and from 2.8 to 7.0‰, respectively. Additionally, the $\delta^{18}O$ and $\delta^{13}C$ isotope values of the two magnesite-rich samples from the TG6 drilling are between 8.1 and 8.8‰ and between −6.7 and −9.5‰, respectively. The $\delta^{13}C$ and $\delta^{18}O$ values of magnesite in all drillings range from −4.8 to −9.5‰ and from 2.3 to 10.5‰, respectively. The $\delta^{13}C$ and $\delta^{18}O$ contents of dolomite in all drillings are slightly lighter than those of magnesite and range from −10.8 to 0.04‰ and from −3.4 to 8.8‰, respectively.

The $\delta^{26}Mg$ values of samples containing dolomite and magnesite from the TG3 drilling range from −0.62 and 0.88‰ (Table 2, Fig. 8).

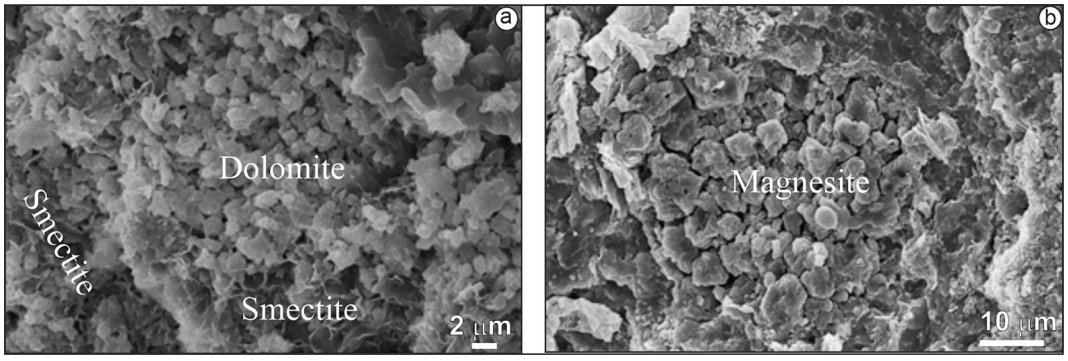

Fig. 7. SEM photos of some samples: a) Mg-rich smectite with subhedral dolomite that precipitated from an Mg-rich solution (TG6 693.6 m). b) Bump-shaped, void-filled magnesite crystals (TG6 332 m).

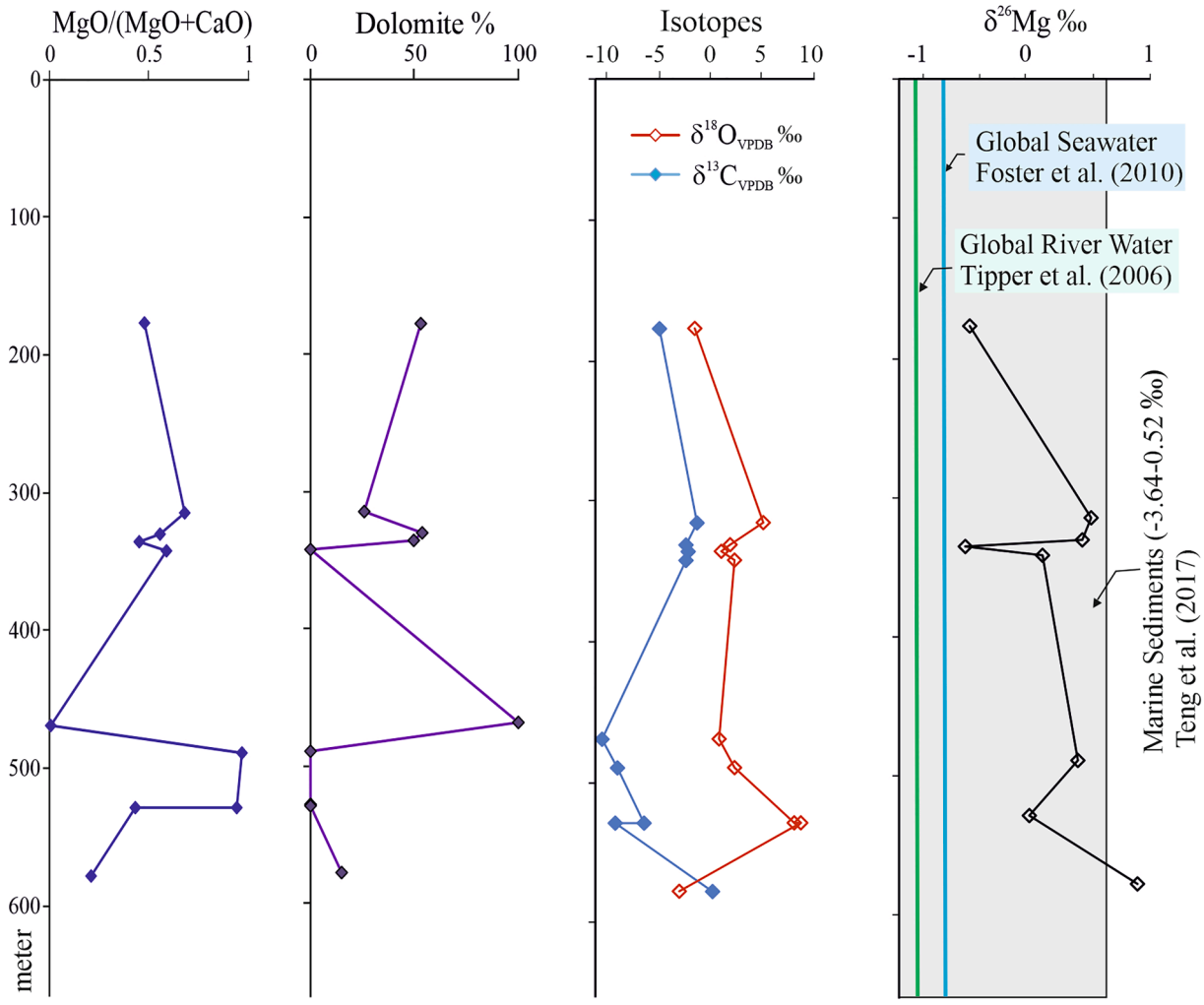

Fig. 8. Variations in $\delta^{26}Mg$, $\delta^{18}O$ and $\delta^{13}C$ values (‰) and semiquantitative dolomite content (% wt.) and MgO/(MgO + CaO) ratios with depth for the TG3 drilling.

5. Discussion

5.1. Precipitation environment of carbonates

Considering the mineralogical composition, textural properties, chemical composition and C, O, and Mg isotope contents of carbonates, the paleodepositional environment, the conditions of the depositional basin, and its origin were discussed under the following subheadings:

5.1.1. Evidence from mineralogical and elemental data

Carbonate minerals (e.g., dolomite and magnesite) were mostly observed as thin bands and cavity fillings or as a matrix between evaporite minerals, which indicates that these carbonates were precipitated before or contemporaneous with the evaporite minerals (Figs. 3–5). The magnesites generally occur as monominerals, whereas dolomite and anhydrite exhibiting microcrystalline properties, fill the gaps between minerals, and show distinctly typical cleavages, and are macroscopically interlaminated (0.1 to 10 cm) with clay and evaporite minerals.

These abovementioned properties indicate that the minerals primarily formed by evaporation and were closely associated with an inland sabkha environment either by marine water entering through permeable rocks (carbonates) or by flooding of marine water into the basin (Warren, 2016). Chicken-wire, entherolithic, grass-like selenite and nodular structures were observed in the dolomitic layer and are typical of synsedimentary to early diagenetic structures formed in sabkha environments (Warren, 2016). Additionally, micron-sized, rounded dolomite crystals are indicative primary precipitation (Fig. 6 d). Mg-smectite, together with dolomite or magnesite, occurs under high-salinity conditions (Warren, 2016).

The high MgO and Sr values of the samples are indicators of paleosalinity and are concentrated in the evaporation phase of waters in closed basins (Gasse et al., 1987). High MgO/(MgO + CaO) ratios, high dolomite contents and high $\delta^{18}O$ values indicate high salinity (Sinha and Smykatz-Kloss, 2003) (Fig. 8). A very weak positive ($r = 0.42$) or lack of correlation is established between the $\delta^{18}O$ values and the MgO/(MgO + CaO), Mg/Ca and Sr/Ca ratios indicating that the basin was partially hydrologically open during the precipitation of carbonate minerals (Sinha et al., 2006). Due to the excessive increase in Mg content in the basin, pure magnesite was formed, suggesting high salinity. Some researchers (Melezhik et al., 2001; Sanz-Montero and Rodriguez-Aranda, 2012; Warren, 2016) pointed out that during carbonate precipitation, Mg^{2+} is enriched in seawater, thus increasing the dolomitization of carbonate muds and the resultant materials could proceed toward magnesite.

In terrestrial evaporites, the Sr contents are generally between 60 and 230 ppm (Krauskopf, 1979), while in marine evaporites, they range from 1200 to 3500 ppm (Emelyanov and Shimkus, 1986; Hasselöv et al., 1999) and 3798 ppm in modern sabkha (Azmy et al., 2013). The Sr values of half of the studied samples are within the range of values given for marine-originated evaporites while the Sr values of almost all the samples are higher than those of terrestrial evaporites. Moreover, the Sr

Table 3
Some major (%) and trace element content (ppm) of the TG3 drilling samples.

Depth Element	Al %	B ppm	Ba ppm	Ca %	Fe %	K %	Li ppm	Mg %	Na %	Rb ppm	SO_4 %	$Si0_2$ %	Sr ppm	Br ppm	Cl %
157	5.01	1153	5557	0.89	0.74	0.19	74	3.53	0.69	74	0.57	57.70	407	146	1.06
163	5.17	1263	47	1.04	1.40	0.41	86	3.51	0.60	86	0.16	60.00	341	1775	1.10
167.7	3.50	1187	41	8.54	2.67	0.66	25	3.64	0.27	25	0.91	50.80	355	1007	0.50
177.3	2.15	1144	30	12.64	1.83	0.76	73	9.85	0.29	73	2.20	29.40	401	473	0.52
183	3.02	1166	229	6.87	2.17	1.07	125	8.29	0.31	125	2.38	46.50	5691	287	0.42
197.7	0.73	1109	82	18.82	0.54	0.24	37	2.40	0.12	37	25.92	1.26	4292	334	0.25
201.5	0.05	701	3	27.09	0.01	0.02	1	0.05	0.00	1	61.31	10.70	192	197	0.01
208	1.44	1318	154	11.70	1.15	0.41	79	7.26	0.47	79	18.78	26.40	8092	140	0.82
213.8	1.22	847	198	14.44	0.93	0.32	71	5.77	0.57	71	18.18	22.90	15,614	178	0.91
228.5	0.59	508	92	19.44	0.52	0.10	34	2.56	0.34	34	50.54	1.56	2750	1199	0.52
251.2	9.31	1436	273	1.91	11.03	2.75	316	13.57	3.54	316	12.32	0.26	1179	301	5.46
273.5	1.30	967	68	20.45	1.07	0.45	68	4.94	0.79	68	49.83	19.70	2708	181	0.85
277.1	1.16	814	94	24.30	0.91	0.36	68	4.69	0.80	68	47.71	17.60	4378	89	1.25
287.8	0.38	385	74	22.41	0.40	0.06	24	1.43	0.32	24	48.23	0.33	3150	291	0.49
291.5	0.67	264	363	2.65	0.73	0.09	126	45.66	2.26	126	4.79	3.06	12,655	1715	3.49
295.3	0.94	1188	95	1.27	0.71	0.24	100	22.47	1.52	100	1.49	18.90	4635	137	2.85
303.7	2.82	987	82	10.42	2.01	0.90	136	4.91	1.33	136	13.25	33.10	2450	70	2.15
312.3	2.92	1007	94	8.84	2.44	1.22	131	6.98	0.86	131	11.13	39.20	2163	82	1.39
315.1	2.79	1089	79	6.50	2.17	0.93	161	11.66	1.18	161	1.11	38.20	1105	87	2.15
328.1	0.75	757	15	19.19	0.68	0.24	151	12.95	1.26	151	0.97	22.90	359	61	2.05
330.2	1.62	788	28	10.72	1.84	0.71	119	11.10	1.33	119	1.79	36.50	190	62	2.11
335.5	0.72	575	58	12.75	1.03	0.22	38	8.90	0.89	38	5.02	25.00	189	108	1.37
336	0.05	321	11	22.79	0.04	0.01	1	0.12	0.05	1	53.15	0.11	256	336	0.08
341.9	0.88	552	41	7.99	1.59	0.27	37	9.85	0.70	37	2.10	36.90	106	67	1.24
346.9	0.01	376	2	27.95	0.00	0.00	1	0.01	0.12	1	62.50	8.39	141	127	0.20
346.9	0.04	316	2	28.93	0.03	0.02	1	0.11	0.02	1	61.66	8.92	226	78	0.04
356.3	0.54	379	33	28.86	0.61	0.16	30	11.26	0.47	30	2.35	11.76	311	86	0.70
359.8	0.43	245	13	34.10	0.47	0.20	15	0.65	0.15	15	52.27	10.38	222	36	0.25
367	0.05	272	9	23.57	0.01	0.35	1	0.02	0.01	1	53.79	0.01	252	293	0.01
367.5	2.54	575	50	10.62	2.50	1.33	100	6.80	1.02	100	9.07	41.50	160	23	1.50
456.8	0.10	260	10	26.23	0.09	0.03	17	13.29	0.25	17	0.87	6.42	923	48	0.43
467.2	0.07	238	2	31.25	0.05	0.03	4	0.25	0.04	4	60.07	6.89	183	40	0.08
479.1	0.68	614	110	9.83	0.58	0.25	69	14.40	0.53	69	11.30	16.30	4794	64	0.99
482.9	0.29	1453	21	6.72	0.32	0.16	118	19.76	0.70	118	9.29	9.76	1693	49	1.12
483.1	1.12	587	27	21.51	1.28	0.57	69	2.85	0.49	69	33.94	24.10	1314	65	0.85
489.3	0.32	578	9	0.92	0.28	0.12	43	25.17	0.72	43	0.61	12.10	1168	66	1.16
501.6	0.02	28	1	0.22	0.03	0.01	1	0.16	39.53	1	0.30	0.09	30	11	59.20
503.3	0.01	326	1	0.07	0.00	0.01	1	8.72	16.51	1	33.93	9.52	14	132	26.52
503.5	0.02	227	2	0.27	0.01	0.03	2	0.22	36.62	2	0.46	7.89	41	17	54.10
504	0.01	181	1	0.09	0.01	0.03	1	2.75	28.16	1	11.37	9.21	14	39	47.80
504.4	0.03	284	1	0.47	0.01	0.03	3	7.05	16.57	3	32.07	11.50	117	66	31.50
507.3	0.49	467	71	10.45	0.43	0.23	37	5.61	11.90	37	29.97	11.60	1940	141	25.20
508.3	0.30	591	39	11.02	0.23	0.15	33	4.49	13.38	33	31.39	8.60	1923	33	28.50
509.6	0.03	19	1	0.14	0.02	0.01	2	0.12	37.73	2	0.23	0.10	65	7	61.59
510.6	0.04	223	6	0.12	0.02	0.02	2	6.56	19.38	2	26.98	1.20	23	88	35.60
511.3	0.01	204	0	0.04	0.01	0.01	2	8.55	16.56	2	36.35	1.20	4	60	38.50
512.5	0.02	213	1	0.06	0.02	0.03	2	0.19	35.74	2	0.20	1.10	18	200	58.50
516	0.56	605	8	11.44	0.50	0.28	31	1.71	13.29	31	33.13	8.10	838	70	25.90
519	0.13	455	3	8.91	0.18	0.07	20	3.30	19.00	20	25.61	1.80	671	90	32.90
527	0.01	11	1	0.28	0.01	0.01	1	0.08	41.03	1	0.65	0.05	35	9	57.66
528.4	0.47	803	107	1.58	0.37	0.16	91	21.70	1.34	91	6.46	3.10	2285	91	2.11
529.2	1.12	315	197	6.74	0.88	0.46	43	3.76	11.92	43	21.31	8.62	683	88	22.90
531.2	0.01	179	1	0.04	0.00	0.01	1	8.48	17.81	1	33.86	1.60	8	22	28.90
533	0.01	183	2	0.18	0.01	0.02	2	5.96	20.93	2	24.15	1.60	53	86	36.50
534	0.03	206	2	0.57	0.03	0.03	3	0.18	33.37	3	1.54	1.60	100	101	60.20
536	0.55	606	8	10.51	0.39	0.37	44	5.17	12.88	44	29.47	4.67	631	46	25.30
537	0.01	13	1	0.22	0.01	0.03	1	0.07	38.57	1	0.53	1.10	34	11	59.54
537.4	0.01	156	1	0.19	0.01	0.04	1	0.06	36.89	1	0.51	3.47	36	38	57.80
549	0.42	286	85	23.52	0.31	0.15	21	0.77	0.19	21	54.84	0.17	1761	66	0.30
555.4	2.21	397	110	8.72	1.74	1.00	66	10.54	0.80	66	7.38	22.90	658	56	1.35
563.8	0.58	173	66	19.92	0.48	0.14	16	2.71	0.29	16	25.91	12.27	1982	30	0.42
567	0.13	230	10	22.59	0.08	0.01	3	0.20	0.03	3	52.02	0.23	237	138	0.04
571.4	0.03	202	6	22.07	0.01	0.01	1	0.02	0.02	1	50.56	0.04	190	37	0.03
577.8	0.19	359	134	25.75	0.18	0.01	29	5.89	0.18	29	36.33	0.74	1119	300	0.27
603.8	2.59	180	60	14.40	2.89	0.94	27	6.07	0.51	27	0.11	29.20	273	136	0.82
612.3	3.39	170	99	12.17	3.11	1.03	27	4.49	0.73	27	0.36	39.70	261	78	1.20
625.4	2.29	111	289	15.04	2.55	0.64	21	5.53	0.40	21	0.08	30.70	343	94	0.65
641	2.97	128	49	10.36	2.37	1.09	38	8.31	0.56	38	0.86	35.00	279	55	0.88
643	3.37	127	58	11.33	3.40	1.04	32	4.18	0.68	32	0.12	35.10	357	87	1.06

values of the many samples are higher than those of marine to hypersaline dolomites (500–800 ppm; Land, 1980) and ancient marine or marine meteoric dolomites (generally < 200 ppm, Oliveri et al., 2010 and reference therein). The high Sr contents of the samples may be sourced from seawater inflowing during the precipitation of celestine (Karakaya et al., 2020). No significant clear relationship was not found between Sr and Ca in the core samples (Table 1, Fig. 9). The late Miocene-Pliocene calc-alkaline volcanism observed among evaporite layers in the study area may have mostly caused the high Sr concentrations. The maximum Sr content was determined to be 4045 ppm in the volcanic rocks (Kadir et al., 2014). Diagenetic crystallization with progressive burial may cause the loss of Sr from the sediment column (Plank and Langmuir, 1998). The Br and Sr contents vary over a very wide range, and their conservative behaviors are used as salinity indicators (Warren, 2016). The Br content of the carbonate-enriched samples is higher than both marine-originated halite (e.g., 60–280 ppm, Petrychenko et al., 2005; 49–77 ppm, Vovnyuk and Czapowski, 2007; 52–191 ppm; García-Veigas et al., 2009) and halites with primary textures, which have the lowest marine Br content (<13 ppm; Salvany et al., 2007). The Br content of carbonate-rich minerals deposited in the same basin with halite is higher than that of marine-originated halite, indicating that seawater fed the basin and that the carbonates are of marine origin. Moreover, the Br, B, Sr, and some Li content are high between 157 and 350 m in the borehole and decrease with depth (Table 3, Fig. 9). The clear enrichment of B, Sr and Li elements at shallow levels compared to deep levels may be related to an increase in the content of clay minerals and volcanic material. The dissolution of the previously precipitated the middle Miocene marine halites may also have caused an increase in Br content in deposits found in the upper level (Ercan et al., 2019; Karakaya et al., 2019, 2020). Therefore, the carbonates deposited simultaneously with evaporites could be from a hypersaline coastal plain environment/lagoon.

5.1.2. *Implications from C and O isotopes*

The carbon isotope values of the carbonate minerals vary over a wide range from −10.78 to 0.04‰. The $\delta^{13}C$ values of half of the TG3 drilling samples are somewhat close to those of marine carbonates (0‰; Veizer et al., 1999 and references therein, and −3 to +3‰, Whitley et al., 2019 and references therein), while the values for other samples from TG3 are considerably lower than marine values and more similar to those of the TG2 and TG6 drilling samples (Table 1, Fig. 8). The slightly negative $\delta^{13}C$ values of dolomite and magnesite (down to −10.8‰) may partially be due to the degradation of organic matter during the carbonate mineral precipitation. $\delta^{13}C$ values can be depleted by up to −22 to −30‰ when if organic substances undergo high amounts of diagenesis (Dela Pierre et al., 2012). The $\delta^{13}C$ values of the studied carbonate minerals are quite higher than the values given by Dela Pierre et al. (2012). Therefore, the slightly negative $\delta^{13}C$ values of the carbonate minerals indicate that the waters in the basin were not subject high organic matter degradation, which would favor the formation of CO_2 of organic origin.

The oxygen isotope values of the carbonate minerals also vary over a wide range from −3.4 to 10.5‰. The $\delta^{18}O$ values of carbonate minerals and other evaporites can be used to explain the effects and changes in climate and water chemistry and to evaluate the paleogeography in the sedimentation area. Oxygen isotope fractionation is principally controlled by evaporation and concentration mechanisms of water at the hydrosphere-atmosphere interface (Horita et al., 1994). Positive $\delta^{18}O$ values indicate that deposition has occurred under evaporative conditions, while partial bacterial sulfate reduction (BSR) processes cause less-negative $\delta^{13}C$ values (Manzi et al., 2011). The presence of carbonate minerals together with other evaporite minerals in the study area and the positive $\delta^{18}O$ values of the studied carbonates show that carbonates precipitated mostly from highly evaporated water. The more positive $\delta^{18}O$ values of the mostly magnesite-enriched samples show that the minerals precipitated in an arid climate and that evaporation processes caused $\delta^{18}O$ enrichment (from −3.4 to 10.4‰). In addition, the enrichment of $\delta^{18}O$ values in the magnesite-rich samples (Fig. 9, Table 1) is also explained by the following mechanisms (Dela Pierre et al., 2012): a) positive $\delta^{18}O$ isotope values of carbonates from the evaporation of seawater and b) flushing of sediments with methane-rich fluids. The presence of bituminous shale and petroleum occurrence at levels usually containing magnesite and/or dolomite at approximately 500 m in all the drillings in the study area indicate the effect of methane-rich fluids. Kralik et al. (1989) published the $\delta^{18}O$ values (from −0.9 to 8.8‰) of magnesites, which are very close to those of the studied carbonate minerals, and explained that the low $\delta^{18}O$ indicate a humid climate while the high $\delta^{18}O$ values signify high salinity.

There is no correlation between the dolomite contents and the $\delta^{18}O$ values of the same samples, while there is a very weak correlation

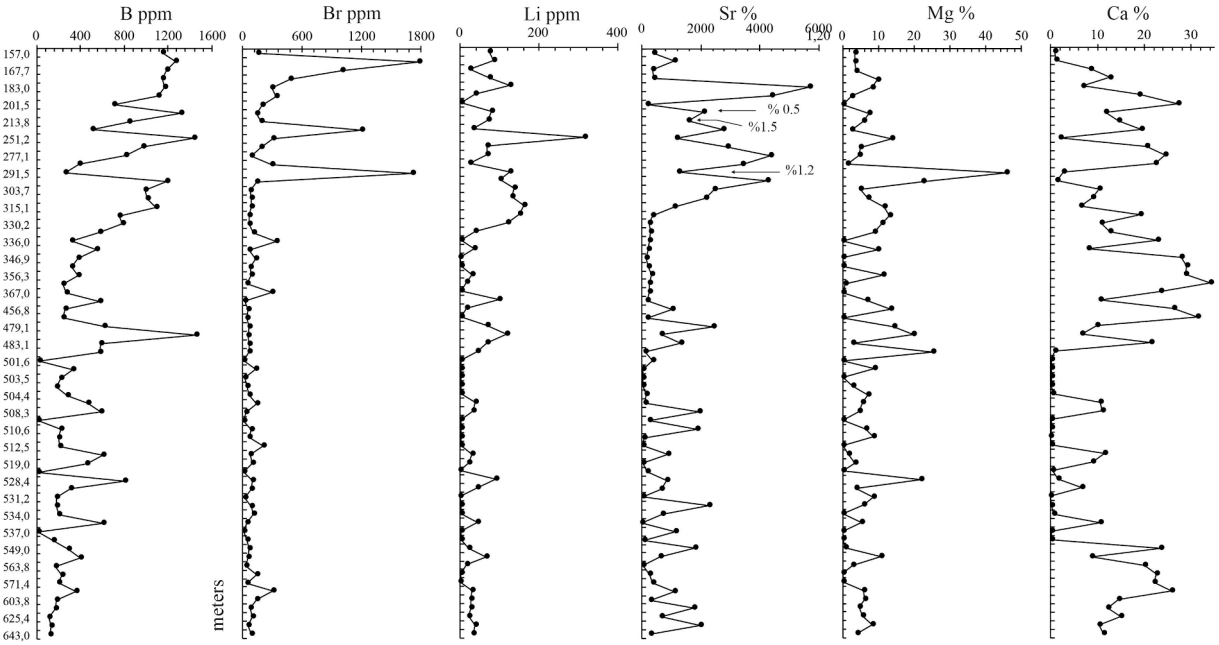

Fig. 9. Variations in some element contents with depth for the TG3 drilling.

between the MgO/(MgO + CaO) ratios and the $\delta^{18}O$ values, which indicates that the basin was partially hydrologically open with seawater intrusion (Fig. 8). For large, closed lake basins, especially in arid zones, both the $\delta^{18}O$ and $\delta^{13}C$ values show high correlations (generally positive) (Leng and Marshall, 2004). There is no significant correlation ($r < 0.35$) between the $\delta^{13}C$ and $\delta^{18}O$ isotope compositions of the carbonates in the Tuz Gölü basin, indicating that they were deposited in a hydrologically open basin (Figs. 8, 10). Talbot (1994) explained that the wide range of $\delta^{13}C$ values combined with relatively limited $\delta^{18}O$ variation is typically characteristic of hydrologically open basins. In addition, Schobben et al. (2016) stated that the presence of a positive relationship between these isotopes indicates partial diagenetic alteration of marine carbonates. Here, both the $\delta^{13}C$ and $\delta^{18}O$ values of the investigated carbonates show wide-ranging variations (e.g., the standard deviations of these isotopes are 3.9 and 3.2‰, respectively). In contrast, modern closed lake carbonates show isotopic variations higher than $r > 0.8$, and thus, Talbot (1994) proposed that the range of $\delta^{18}O$ values and degree of covariance can be used to distinguish between hydrologically open and closed lake basins. The $\delta^{18}O$ and $\delta^{13}C$ values of the studied dolomite and magnesite samples in the present study fall neither in the closed lake nor open lake areas defined by Talbot (1994), and do not show diagenetic alteration (Fig. 10). Most of the samples show high $\delta^{18}O$ and low $\delta^{13}C$ values, and a few samples fall in the range of marine dolomite areas defined by Geske et al. (2015). Therefore, the O and C isotope compositions may indicate that the carbonates were precipitated in environments such as lagoonal, subtidal or estuarine environment exposed to seawater incursion. According to the $\delta^{18}O$ and $\delta^{13}C$ values on the graph of Manzi et al. (2011) (Fig. 11), the positive $\delta^{18}O$ values that fall in the open marine and evaporative areas on the graph (Fig. 11) indicate that precipitation was occurred by the strong evaporation of seawater in the environment, while incomplete BSR processes caused less negative $\delta^{13}C$ values (Manzi et al., 2011).

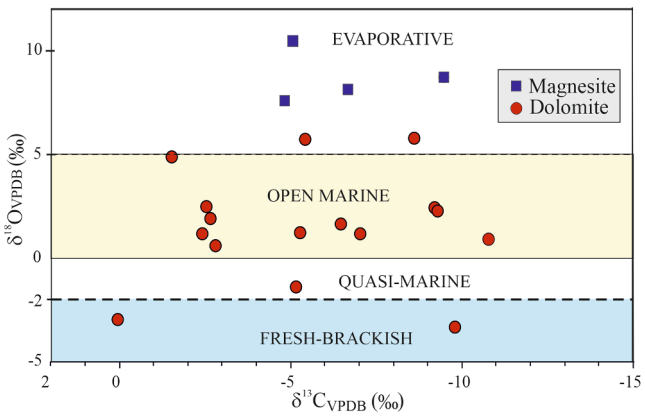

Fig. 11. Diagram showing paleoenvironments (after Manzi et al., 2011) of the carbonates using $\delta^{18}O$ and $\delta^{13}C$ values from the TG2, TG3 and TG6 drillings.

5.1.3. Mg Isotopic record of the carbonates: Evidence of seawater incursion

The $\delta^{26}Mg$ values of the studied samples can be divided into two groups; the first group has negative values between −0.62 and −0.07‰ and the second group has more positive $\delta^{26}Mg$ values between 0.05 and 0.88‰ (Table 2). The negative values are very close to the $\delta^{26}Mg$ values (−0.82 ± 0.06‰, n = 26, Foster et al., 2010) for current marine conditions. The $\delta^{26}Mg$ values change within a narrow range and most of these values are within the range of the values given for marine sediments (−3.65 to +0.52‰; Teng, 2017) (Fig. 8). The $\delta^{26}Mg$ values of the all samples display a positive correlation ($r = 0.80$; dolomite containing samples: $r = 0.90$) with the MgO content, indicating that Mg-enriched water was present during carbonate precipitation. Magnesium isotope compositions have been investigated in many studies as a paleo-climatic

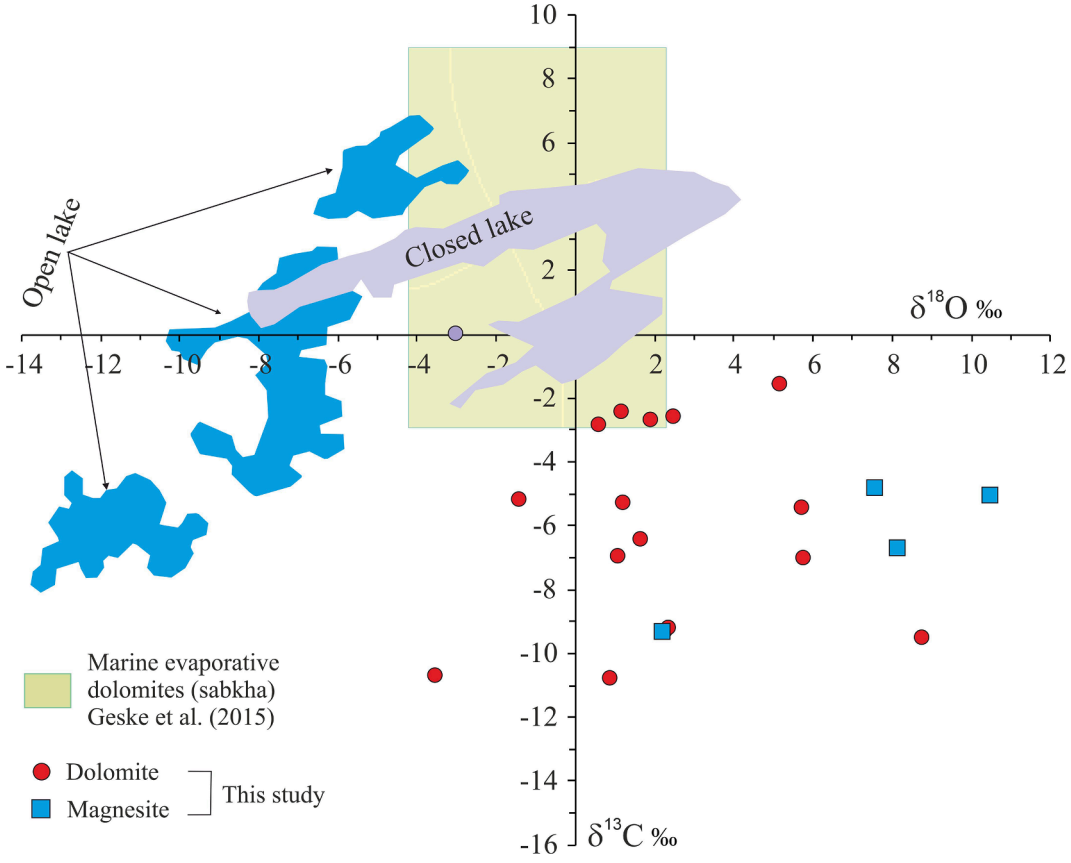

Fig. 10. $\delta^{18}O$ and $\delta^{13}C$ values of the studied dolomite and magnesite samples (Table 1), and areas of open and closed lakes were modified from Talbot (1994).

markers for both marine and non-marine environments (Li et al., 2012 and references therein; Teng, 2017 and references therein). In addition, Mg isotope fractionations in evaporitic deposits provide information regarding the openness of the system, paleo-moisture levels and paleo-hydrological aspects of the environments (Foster et al., 2010; Li et al., 2011; Geske et al., 2015; Meng et al., 2019 and references therein). Magnesium can be sourced from mostly magmatic (mainly mafic to ultramafic rocks), hydrothermal, or sedimentary sources (dolostone and Mg-rich clays). Sedimentary carbonate rocks have variable Mg isotope values that are lower than those of igneous rocks while limestones sedimentary dolostones and marlstones usually show more negative δ^{26}Mg values (δ^{26}Mg < −2.5‰) (Meng et al., 2019 and references therein). In addition, Geske et al. (2015) stated that the δ^{26}Mg values of dolostones showed a relatively broad range (−2.49 to −0.45‰; mean = −1.75 ± 1.08‰, n = 42), whereas the δ^{26}Mg values of normal marine sedimentary dolostones ranged from −2.29 to −1.09‰. Ma et al. (2015) explained that chemical decomposition of shales can cause significant fractionation of Mg isotopes. Teng (2017) reported that carbonate-rich sediments are generally enriched in light Mg isotopes, while silicate minerals are enriched with heavy Mg isotopes. In the studied samples, the lack of a significant increase in Mg isotope values at deeper levels of drilling and a close-to-one correlation (r = 0.99) between light Mg and heavy Mg isotopes may indicate that carbonate or silicate minerals in the basin did not affect these isotope values. Additionally, the absence of a significant increase in Mg isotope values at deep levels of drilling may indicates that the diagenetic effect is not significant while increased evaporation in the basin and precipitation of halite and sulfate minerals may have caused an increase in the Mg content and the occurrence of partially inhomogeneous isotope values.

Crystallization of the sulfate minerals (gypsum/anhydrite) commonly found in the basin (Karakaya et al., 2020) increased the Mg/Ca ratio and resulted in the formation of Mg-enriched solutions (brines), subsequently leading to magnesite precipitation. Water interactions with basement rocks (ultramafic rocks and dolomitic limestones) may also have affected the Mg^{2+} content and, therefore, the enrichment of δ^{26}Mg in the solution. In addition, the clay content (especially Mg-smectite and sepiolite minerals) and diagenesis represent another effective geological mechanism that causes enrichment of δ^{26}Mg values in the basin. The δ^{26}Mg values of the investigated samples are higher than those from the global mean values of rivers (−1.09‰; Tipper et al., 2006). In addition, rivers draining carbonates usually have lighter Mg isotopic compositions than those draining silicates while low δ^{26}Mg values (between −1.70 and −1.18‰) were determined in groundwater where carbonate rocks are common (Teng, 2017). The Cambrian to Tertiary basement rocks (Central Taurus) in the eastern and southern parts of the Tuz Gölü Basin are generally composed of carbonate, ophiolites and sedimentary- metasedimentary rocks formed in shelf environments (Demirtaşlı et al., 1984; Fig. 1b). The measured Mg isotope values indicate that the effects of rivers and groundwater draining from the carbonate rocks in question were quite weak. Since the δ^{26}Mg values of the seawater in the Middle Miocene were nearly constant (~ 0‰; Pogge von Strandmann et al., 2014) and the δ^{26}Mg values of rivers (−1.09‰) and δ^{26}Mg values of basement rocks (e.g., carbonates and ultramafics) (−0.25‰, Meng et al., 2019) were low, the δ^{26}Mg values of the samples in the Tuz Gölü Basin may have been affected by decomposition of detrital sediments containing Mg-rich minerals and may also have been linked to marine water. Similarly, Gothmann et al. (2017) reported that the increase in the Mg content of seawater in the Cenozoic was mainly due to an increase in Mg-silicate decomposition or a decrease in Mg uptake in marine silicates. The researchers also proposed that changes in the rate of carbonate decomposition and dolomite formation likely played a minor but not insignificant role in the global Mg cycle in the Cenozoic. Additionally, Pogge von Strandmann et al. (2020) reported that weathering is the primary source of Mg in oceans, and smectites and most of other secondary silicates preferably take up heavy Mg isotopes, while the remaining waters are isotopically light. In summary, the contribution of seawater, which caused increased δ^{26}Mg values in the basin, may have led to more positive δ^{26}Mg values because the isotopic values of seawater are always heavier than those of river water (Fan et al., 2016). Furthermore, many researchers have reported that the Mg isotopic variation is not related to the age or type of dolostones but is mainly related to changes in the Mg isotopic composition of fluids, dolomite-fluid fractionation factors and diagenesis (Geske et al., 2015; Teng, 2017 and reference therein). The variations in the Mg isotopic values of the Tuz Gölü samples may be related to different diagenetic processes (burial effect), the alteration of source rocks and variation in the Mg sources during precipitation processes.

The presence of marine water contributions to the precipitation of evaporites in the Tuz Gölü basin has also been supported by various isotope (δ^{7}Li, δ^{11}B, δ^{18}O, δ^{34}S, δ^{37}Cl, δ^{81}Br, and ^{87}Sr/^{86}Sr) results and element contents in halites and sulfates (Ercan et al., 2019; Karakaya et al., 2019, 2020). In the southern part of the CAP, during the evaporite deposition period, the mixing of sea water into the basin is related to the fact that the topography at that time is different from today (Fig. 12). Öğretmen et al. (2018) declared that most of the topographic altitude, which reaches up to 2 km today and is an important barrier separating the study area from the Mediterranean, forms the southern boundary of the CAP including the study area, and does not occur before 5 Ma.

All isotopic (C, O and Mg) data, geochemical, mineralogical, lithological results and previously determined diatom species in the study area showed that the studied region was a shallow-water environment, e.g., lagoon, estuary, subtidal and marsh environments, which are mostly environments where seawater incursion is effective, and show hydrologically open basin properties (Fig. 12). In addition, Schildgen et al. (2012b) stated that the southern part of the Mediterranean, including the study area, was below sea level and that marine sediments were deposited in many basins prior to 8 Ma (Fig. 1). In the study area, nonevaporitic sediments were deposited during the period when sea water flooded the basin, and evaporites were deposited during the periods when the sea water withdrew. During the withdrawal periods arid conditions were effective and evaporites were deposited (Fig. 12). Therefore, the trapped seawater in the basin played an important role in the origin of the precipitated evaporite minerals. Furthermore, Hüsing et al. (2009) stated that approximately 11 Ma is the youngest possible age for a deep marine connection between the Mediterranean-Atlantic and Indo-Pacific regions. In addition, Boulton and Robertson (2007) reported in their study performed in the southern region of Turkey that during the middle Miocene, tectonic subsidence during a time of sea-level rise favored the deposition of shallow-marine carbonates on an overall northward-deepening carbonate ramp, with lagoons and reefs developed locally. Hence, the previously published results of some researchers (Karakaya et al., 2019, 2020; Ercan et al., 2019) and the findings of other researchers (Boulton and Robertson 2007; Hüsing et al., 2009; Schildgen et al., 2012b) coincide with the data obtained in the present study.

6. Conclusion

The main results obtained in this study are summarized below:

1. The high variations in both δ^{13}C and δ^{18}O values and the lack of a correlation between δ^{18}O values and MgO/(MgO + CaO), Mg/Ca and Sr/Ca ratios may indicate that the investigated evaporite deposits were precipitated in a lagoon environment exposed to seawater incursions.
2. The low δ^{13}C values (−10 to 0.04 ‰) and high δ^{18}O values (−3.4 to 10.5 ‰), lack of covariance between the isotopes, and the presence of indicative evaporite minerals indicate the presence of arid conditions during the regressions.
3. The δ^{18}O values of both dolomite- and magnesite-bearing samples reveal that the carbonate precipitated from fluids mainly derived

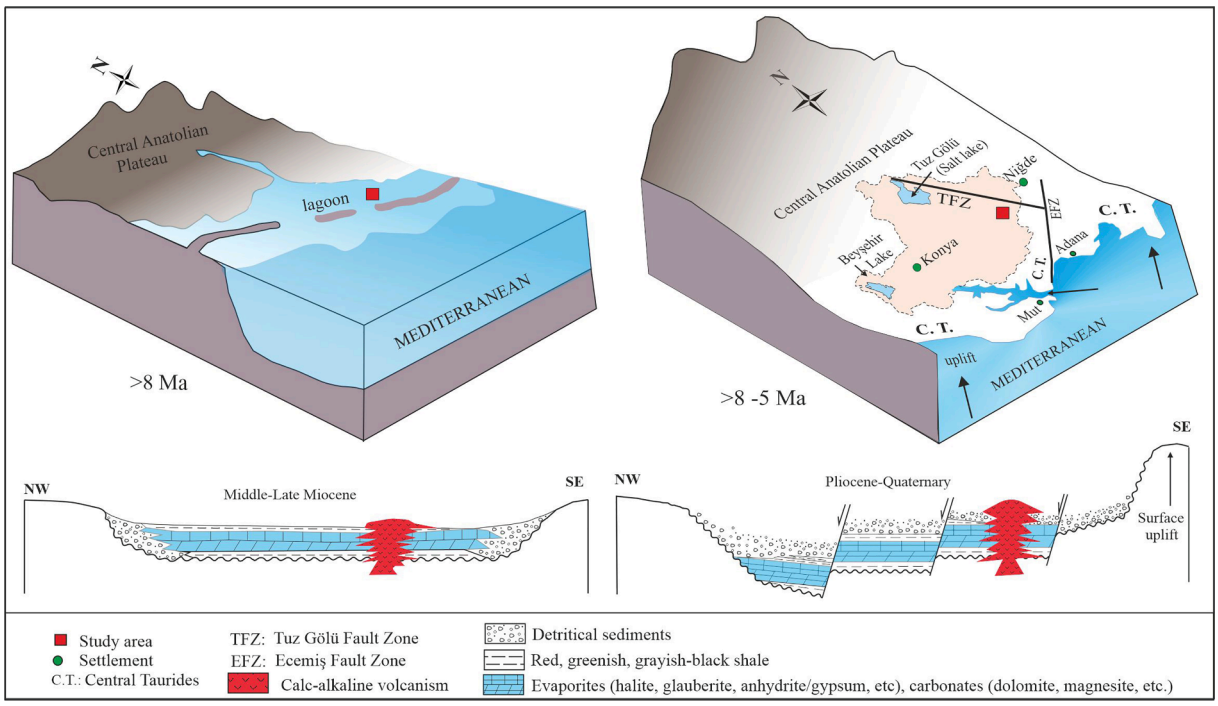

Fig. 12. Conceptional figures showing the mid-late Miocene lithofacies and paleoceography of the study area and southern parts of Anatolia.

from seawater and evaporation was intense when seawater was withdrawn from the basin.

4. The Mg isotope compositions of carbonates indicate of seawater incursions into the basin.
5. Moreover, mineralogical, elemental, and isotopic data of the study indicate that the MSC causing the formation of the middle to late Miocene deposits in the southern coast of Turkey may have also affected the formation of the studied evaporites.

Declaration of Competing Interest

The authors declare that they have no known competing financial interests or personal relationships that could have appeared to influence the work reported in this paper.

Acknowledgement

This research was made possible with the support of The Scientific and Technological Research Council of Turkey (TÜBİTAK 114Y629) and partly the Selçuk University Scientific Research Projects support program (17201027 project). We also thanks to MTA for helping us obtain the drilling samples, and Prof. Dr. Faruk Ocakoğlu and the anonymous reviewer for constructive recommendations, and American Journal Experts for editing the manuscript.

References

Akgün, F., Kayseri-Özer, M.S., Tekin, E., Varol, B., Şen, Ş., Herece, E., Gündoğan, İ., Sözeri, K., Us, S.M., 2020. Late Eocene to Late Miocene palaeoecological and palaeoenvironmental dynamics of the Ereğli-Ulukışla Basin (Southern Central Anatolia). Geol. J. 1–31. https://doi.org/10.1002/gj.4021.

Aksu, A.E., Hall, J., Calon, T.J., Barnes, M.C., Güneş, P., Cranshaw, J.C., 2018. Messinian evaporites across the Anaximander Mountains, Sırrı Erinç Plateau and the Rhodes and Finike basins, eastern Mediterranean Sea. Mar. Geol. 395, 48–64.

Aydar, E., Schmitt, A.K., Çubukçu, H.E., Akin, L., Ersoy, O., Sen, E., Duncan, R.A., Atici, G., 2012. Correlation of ignimbrites in the central Anatolian volcanic province using zircon and plagioclase ages and zircon compositions. J. Volcanol. Geoth. Res. 213-214, 83–97.

Azmy, K., Lavoie, D., Wang, Z., Brand, U., Al-Aasm, I., Jackson, S., Girard, I., 2013. Magnesium isotope and REE composition of Lower Ordovician carbonates from eastern Laurentia: Implications for the origin of dolomites and limestones. Chem. Geol. 356, 64–75.

Bassant, P., Van Buchem, F.S.P., Strasser, A., Görür, N., 2005. The stratigraphic architecture and evolution of the Burdigalian carbonate-siliciclastic sedimentary systems of the Mut Basin, Turkey. Sed. Geol. 173 (1-4), 187–232.

Boulton, S.J., Robertson, A.H.F., 2007. The Miocene of the Hatay area, S Turkey: Transition from the Arabian passive margin to an underfilled foreland basin related to closure of the southern Neotethys Ocean. Sed. Geol. 198 (1-2), 93–124. https://doi.org/10.1016/j.sedgeo.2006.12.001.

Cipollari, P., Halásová, E., Gürbüz, K., Cosentino, D., 2013. Middle-Upper Miocene paleogeography of southern Turkey: Insights from stratigraphy and calcareous nannofossil biochronology of the Olukpınar and Başyayla sections (Mut-Ermenek Basin). Turk. J. Earth Sci. 22, 820–838. https://doi.org/10.3906/yer-1208-2.

Cosentino, D., Schildgen, T.F., Cipollari, P., Faranda, C., Gliozzi, E., Hudackova, N., Lucifora, S., Strecker, M.R., 2012. Late Miocene surface uplift of the southern margin of the Central Anatolian plateau, Central Taurides, Turkey. Geol. Soc. Am. Bull. 124 (1-2), 133–145. https://doi.org/10.1130/B30466.1.

Ćorić, S., Harzhauser, M., Rögl, F., İslamoğlu, Y., Landa, B., 2012. Biostratigraphy of some mollusc-bearing middle Miocene localities on the Karaman high plain (Turkey, Konya Province). Cenozoic Res. 9, 281–288.

Çemen, I., Göncüoğlu, M., Dirik, K., 1999. Structural evolution of the Tuzgolu Basin in Central Anatolia, Turkey. J. Geol. 107, 693–706.

Dela Pierre, F., Pierangelo, C., Bernardi, E., Natalicchio, M., Costa, E., Cavagna, S., Lozar, F., Lugli, S., Manzi, V., Roveri, M., Violanti, D., 2012. Messinian carbonate-rich beds of the Tertiary Piedmont Basin (NW Italy): microbially-mediated products straddling the onset of the salinity crisis. Palaeogeogr. Palaeoclimatol. Palaeoecol. 344–345, 78–93.

Demirtaşlı, E., Turhan, N., Bilgin, A.Z., Selim, M., 1984. Geology of the Bolkar Mountains. In: Tekeli, O., Göncüoğlu, M.C. (Eds.), Geology of the Taurus Belt. Maden Tetkik ve Arama Enstitüsü, Ankara, Turkey, pp. 125–141.

Dirik, K., 2001. Neotectonic evolution of the northwestward arched segment of the Central Anatolian Fault Zone, Central Anatolia, Turkey. Geodin. Acta 14 (1-3), 147–158.

Dirik, K., Erol, O., 2000. Tuzgölü ve civarının tektonomorfolojik evrimi Orta Anadolu, Türkiye, Haymana-Tuzgölü-Ulukışla Basenleri Uygulamalı Çalışma (Workshop), T.P. J.D. Bülteni (Turkish with English abstract).

Dirik, K., Erol, O., 2003. Tectonomorphologic evolution of Tuzgölü and surrounding area, central Anatolia-Turkey. Turk Assoc. Petroleum Geolog. Special Publ. 5, 27–46.

Emelyanov, E.M., Shimhus, K.M., 1986. Geochemistry and sedimentology of the Mediterranean Sea. 176p. Paris.

Epstein, S., Buchsbaum, H.A., Lowenstam, Urey, H.C., 1953. Revised carbonate-water isotopic temperature scale. Geol. Soc. Am. Bul. 64, 1315–1325.

Ercan, H.Ü., Karakaya, M.Ç., Bozdağ, A., Karakaya, N., Delikan, A., 2019. Origin and evolution of the halite based on stable isotopes ($\delta^{37}Cl$, $\delta^{81}Br$, $\delta^{11}B$ and $\delta^{7}Li$) and trace elements in Tuz Gölü Basin, Turkey. Appl. Geochem. 105, 17–30.

Fan, B., Zhao, Z.-Q., Tao, F., Li, X., Tao, Z., Gao, S., He, M., 2016. The geochemical behavior of Mg isotopes in the Huanghe basin, China. Chem. Geol. 426, 19–27.

Fernández-Blanco, D., Bertotti, G., Çiner, T.A., 2013. Cenozoic tectonics of the Tuz Gölü Basin (Central Anatolian plateau, Turkey). Turk. J. Earth Sci. 715–738.

Foster, G.L., Pogge von Strandmann, P.A.E., Rae, J.W.B., 2010. The boron and magnesium isotopic composition of seawater. Geochem. Geophys. Geosyst. 11, Q08015. https://doi.org/10.1029/2010GC003201.
Flügel, E., 2004. Microfacies of carbonate rocks: analysis, interpretation and application. Springer Science & Business Media.
García-Veigas, J., Rosell, L., Zak, I., Playà, E., Ayora, C., Starinsky, A., 2009. Evidence of potash salt formation in the Pliocene Sedom Lagoon (Dead Sea Rift, Israel). Chem. Geol. 265 (3-4), 499–511.
Gasse, F., Fontes, J.C., Plaziat, J.C., Carbonel, P., Kaczmarska, I., De Deckker, P., Soulié-Marsche, I., Callot, Y., Dupeuble, P.A., 1987. Biological remains, geochemistry and stable isotopes for the reconstruction of environmental and hydrological changes in the Holocene lakes from North Sahara. Palaeogeogr. Palaeoclimatol. Palaeoecol. 60, 1–46.
Geske, A., Goldstein, R.H., Mavromatis, V., Richter, D.K., Buhl, D., Kluge, T., John, C.M., Immenhauser, A., 2015. The magnesium isotope (δ^{26}Mg) signature of dolomites. Geochim. Cosmochim. Acta 149, 131–151.
Gothmann, A.M., Stolarski, J., Adkins, J.F., Higgins, J.A., 2017. A Cenozoic record of seawater Mg isotopes in well-preserved fossil corals. Geology 45, 1039–1042. https://doi.org/10.1130/g39418.1.
Gündoğdu, M.N., 1982. Neojen yaşlı Bigadiç sedimanter baseninin jeolojik, mineralojik ve jeokimyasal incelenmesi. PhD thesis. Hacettepe University, Ankara, Turkey, p. 386 pp..
Güneş, P., Aksu, A.E., Hall, J., 2018. Internal seismic stratigraphy of the Messinian evaporites across the northern sector of the eastern Mediterranean Sea. Mar. Pet. Geol. 91, 297–320.
Gürbüz, A., Kazancı, N., 2014. Facies characteristics and control mechanisms of Quaternary deposits in the Lake Tuz Basin: Bulletin of the Mineral. Res. Explorat. 149, 1–18.
Hasselöv, M., Lyven, D., Haraldsson, C., Sirnawin, W., 1999. Determination of continuous size and trace element distribution of field flow fractionation with ICP-MS. Anal. Chem. 71, 3497–3502.
Horita, J., Cole, D.R., Wesolowski, D.J., 1994. Salt effects on stable isotope partitioning and their geochemical implications for geothermal brines. In: Proceedings: Nineteenth Workshop on Geothermal Reservoir Engineering, pp. 285–290.
Hüsing, S.K., Kuiper, K.F., Link, W., Hilgen, F.J., Krijgsman, W., 2009. The upper Tortonian–lower Messinian at Monte dei Corvi (Northern Apennines, Italy): completing a Mediterranean reference section for the Tortonian Stage. Earth Planet. Sci. Lett. 282 (1–4), 140–157.
Ilgar, A., Nemec, W., Hakyemez, A., Karakuş, E., 2013. Messinian forced regressions in the Adana Basin: a near-coincidence of tectonic and eustatic forcing. Turk. J. Earth Sci. 22, 864–889.
Kadınkız, G., Pekgöz, M., Karakaş, M., Murat, A., 2017. Sodium sulfate (Glauberite-Bloedite)-Halite association in the tertiary (upper Miocene-Pliocene) Katrandedetepeformation, Ereğli-Bor basin, Turkey. Bull. Mineral Res. Explorat. 154, 135–156.
Kadir, S., Külah, T., Eren, M., Önalgil, N., Gürel, A., 2014. Mineralogical and geochemical characteristics and genesis of the Güzelyurt alunite-bearing kaolinite deposit within the Late Miocene Gördeles ignimbrite, central Anatolia, Turkey. Clays Clay Miner. 62 (6), 477–499.
Karakaya, M.Ç., Bozdağ, A., Ercan, H.Ü., Karakaya, N., Delikan, A., 2019. Origin of Miocene halite from Tuz Gölü basin in Central Anatolia, Turkey: Evidences from the pure halite and fluid inclusion geochemistry. J. Geochem. Explor. 202, 1–12.
Karakaya, M.Ç., Bozdağ, A., Ercan, H.Ü., Karakaya, N., 2020. The origin of Miocene evaporites in the Tuz Gölü basin (Central Anatolia, Turkey): implications from strontium, sulfur and oxygen isotopic compositions of the Ca-sulfate minerals. Appl. Geochem. 120, 104682. https://doi.org/10.1016/j.apgeochem.2020.104682.
Koç, A., Kaymakci, N., Van Hinsbergen, D.J.J., Kuiper, K.F., 2017. Miocene tectonic history of the Central Tauride intramontane basins, and the paleogeographic evolution of the Central Anatolian Plateau. Global Planet. Change 158, 83–102.
Kralik, M., Aharon, P., Schroll, E., Zachmann, D., 1989. Carbon and oxygen isotope systematics of magnesites: a review. In: P. Motler (Ed.), On the formation of magnesite. Monograph Sen Mineral Dep. Borntraeger, vol. 28, pp. 97–224.
Krauskopf, K.B., 1979. Introduction to Geochemistry. McGraw-Hill-Kogakusha, Tokyo, p. 617.
Kürçer, A., Gökten, Y.E., 2014. Neotectonic-period characteristics, seismicity, geometry and segmentation of the Tuz Gölü fault zone. Bull Min Res Exp 149, 19–68.
Land, L.S. 1980. The isotopic and trace element geochemistry of dolomite: the state of the art. In: Zenger, D.H., Ethington, R.L. (Eds.), Concept and Models of Dolomitization. Society of Economic Paleontologists and Mineralogists, Special Publications, vol. 28, pp. 87–110.
Leng, M.J., Marshall, J.D., 2004. Palaeoclimate interpretation of stable isotope data from lake sediment archives. Quat. Sci. Rev. 23, 811–831.
Li, W., Beard, B.L., Johnson, C.M., 2011. Exchange and fractionation of Mg isotopes between epsomite and saturated $MgSO_4$ solution. Geochim. Cosmochim. Acta 75, 1814–1828.
Li, W., Chakraborty, S., Beard, B.L., Romanek, C.S., Johnson, C.M., 2012. Magnesium isotope fractionation during precipitation of inorganic calcite under laboratory conditions. Earth Planet. Sci. Lett. 333 (334), 304–316.
Ma, L., Teng, F.-Z., Jin, L., Ke, S., Yang, W., Gu, H.-O., Brantley, S.L., 2015. Magnesium isotope fractionation during shale weathering in the Shale Hills Critical Zone Observatory: Accumulation of light Mg isotopes in soils by clay mineral transformation. Chem. Geol. 397, 37–50.
Manzi, V., Gennari, R., Lugli, S., Roveri, M., Schreiber, B.C., 2011. The Messinian "Calcare di Base" (Sicily, Italy) revisited. Geol. Soc. Am Bull. 123, 347–370.
McNab, F., Ball, P.W., Hoggard, M.J., White, N.J., 2018. Neogene uplift and magmatism of Anatolia: Insights from drainage analysis and basaltic geochemistry. Geochem. Geophys. Geosyst. 19, 175–213. https://doi.org/10.1002/2017GC007251.
Meijers, M.J.M., Brocard, G.Y., Whitney, D.L., Mulch, A., 2020. Paleoenvironmental conditions and drainage evolution of the central Anatolian lake system (Turkey) during late Miocene to Pliocene surface uplift. Geosphere 16 (X), 1–20.
Melezhik, V.A., Gorokhov, I.M., Kuznetsov, A.B., Fallick, A.E., 2001. Chemostratigraphy of Neoproterozoic carbonates: Implications for 'blind dating'. Terra Nova 13 (1), 1–11.
Meng, J., Li, H., Li, Y., Zhang, Z., Li, L., Song, Z., 2019. Stable isotope (S, Mg, B) constraints on the origin of the early Precambrian Zhaoanzhuang serpentine-magnetite deposit. southern North China Craton Minerals 9, 1–33. https://doi.org/10.3390/min9060377.
Oktay, F., 1982. Ulukışla ve çevresinin stratigrafisi ve jeolojik evrimi, Türkiye Jeoloji Kurumu Bülteni 25, 15-24 ((Turkish with English abstract)).
Oliveri, E., Neri, R., Bellanca, A., Riding, R., 2010. Carbonate stromatolites from a Messinian hypersaline setting in the Caltanissetta Basin, Sicily: petrographic evidence of microbial activity and related stable isotope and rare earth element signatures. Sedimentology 57, 142–161.
Öğretmen, N., Cipollari, P., Frezza, V., Faranda, C., Karanika, K., Gliozzi, E., Cosentino, D., 2018. Evidence for 1.5 km of uplift of the Central Anatolian Plateaus southern margin in the last 450 kyr and implications for its multiphased uplift history. Tectonics 37, 359–390.
Özsayın, E., Dirik, K., 2007. Quaternery activity of the Cihanbeyli and Yeniceoba Fault Zones: İnönü-Eskişehir Fault System, Central Anatolia. Turk. J. Earth Sci. 16, 471–492.
Özsayın, E., Çiner, A., Rojay, B., Dirik, K., Melnick, D., Fernandez-Blanco, D., Bertotti, G., Schildgen, T.F., Garcin, Y., Strecker, M.R., Sudo, M., 2013. Plio-Quaternary Extensional Tectonics of the Central Anatolian Plateau: A case study from the Tuz Gölü Basin, Turkey. Turkish J. Earth Sci. https://doi.org/10.3906/yer-1210-5.
Petrychenko, Peryt, O.Y., Chechel, T.M.E.I., 2005. Early Cambrian seawater chemistry from fluid inclusions in halite from Siberian evaporites. Chem. Geol. 219, 149–161.
Plank, T., Langmuir, C.H., 1998. The chemical composition of subducting sediment and its consequences for the crust and mantle. Chem. Geol. 145 (3-4), 325–394.
Pogge von Strandmann, P.A.E., Forshaw, J., Schmidt, D.N., 2014. Modern and Cenozoic records of seawater magnesium from foraminiferal Mg isotopes. Biogeosciences 11, 5155–5168.
Pogge von Strandmann, P.A.E., Burton, K.W., Opfergelt, S., Eiríksdóttir, E.S., Murphy, M. J., Einarsson, A., Gislason, S.R., 2020. Hydrothermal and Cold Spring Water and Primary Productivity Effects on Magnesium Isotopes: Lake Myvatn, Iceland. Front. Earth Sci. 8, 1–12. https://doi.org/10.3389/feart.2020.00109.
Salvany, JM., García-Veigas, J., Ortí, F., 2007. Glauberite-halite association of the Zaragoza gypsum formation (Lower Miocene, Ebro Basin, NE Spain). Sedimentology 54 (2), 443–467.
Sanz-Montero, M.E., Rodríguez-Aranda, J.P., 2012. Magnesite formation by microbial activity: Evidence from a Miocene hypersaline lake. Sed. Geol. 263-264, 6–15.
Schildgen, T.F., Cosentino, D., Bookhagen, B., Niedermann, S., Yildirim, C., Echtler, H.P., Wittmann, H., Strecker, M.R., 2012a. Multi-phase uplift of the southern margin of the Central Anatolian plateau: a record of tectonic and upper mantle processes. Earth Planet. Sci. Lett. 317–318, 85–95.
Schildgen, T.F., Cosentino, D., Caruso, A., Buchwaldt, R., Yıldırım, C., Bowring, S.A., Rojay, B., Echtler, H., Strecker, M.R., 2012b. Surface expression of eastern Mediterranean slab dynamics: Neogene topographic and structural evolution of the southwest margin of the Central Anatolian Plateau, Turkey. Tectonics 31 (2). https://doi.org/10.1029/2011TC003021.
Schildgen, T.F., Cosentino, D., Frijia, G., Castorina, F., Dudas, F.O., Iadanza, A., Sampalmieri, G., Cipollari, P., Caruso, A., Strecker, M.R., 2014. Sea level and climate forcing of the Sr isotope composition of late Miocene Mediterranean marine basins. Geochem. Geophys. Geosyst. 15, 2964–2983.
Schumacher, R., Keller, J., Bayhan, H., 1990. Depositional characteristics of ignimbrites in Cappadocia, Central Anatolia, Turkey. In: Savaşçın, M.Y., Eronat, A.H. (Eds.), Proceedings of the International Earth Sciences Congress on Aegean Regions, pp. 435–449.
Schobben, M., Ullmann, C.V., Leda, L., Korn, D., Struck, U., Reimold, W.U., Ghaderi, A., Algeo, T.J., Korte, C., 2016. Discerning primary versus diagenetic signals in carbonate carbon and oxygen isotope records: an example from the Permian-Triassic boundary of Iran. Chem. Geol. 422, 94–107.
Sinha, R., Smykatz-Kloss, W., 2003. Thermal characterization of lacustrine dolomites from the Sambhar lake playa, Thar Desert, India. J. Therm. Anal. Calorim. 71, 739–750.
Sinha, S.K., Kumar, L., Srivastava, R., Thangamani, R.,Kumar, S., Jha, S.,Kuthra, P.K., Ashutosh, P., 2006. Evaporation Control in Reservoirs Central Water Commission of India, Basin Planning and Management Organization, New Delhi, India, pp. 96.
Talbot, M.R., 1994. A review of the palaeohydrological interpretation of carbon and oxygen isotopic ratios in primary lacustrine carbonates. Chem. Geol. (Isotope Geosc. Section) 80 (4), 261–279.
Şafak, Ü., Kelling, G., Gökçen, N.S., Gürbüz, K., 2005. The mid-Cenozoic succession and evolution of the Mut basin, southern Turkey, and its regional significance. Sed. Geol. 173, 121–150. https://doi.org/10.1016/j.sedgeo.2004.03.012.
Tekin, E., Ayyıldız, T., Gündoğan, Orti, F., 2007. Modern halolites (halite oolites) in the Tuz Gölü, Turkey. Sedimentary Geol. 195, 101–112.
Tekin, E., Varol, B., Ayyıldız, T., 2010. Sedimentology and paleoenvironmental evolution of Messinian evaporites in the Iskenderun-Hatay basin complex, southern Turkey. Sed. Geol. 229, 282–298.
Teng, F.Z., 2017. Magnesium isotope geochemistry. Rev. Mineral. Geochem. 82, 219–287. https://doi.org/10.2138/rmg.2017.82.7.

Tipper, E.T., Galy, A., Gaillardet, J., Bickle, M.J., Elderfield, H., Carder, E.A., 2006. The magnesium isotope budget of the modern ocean: constraints from riverine magnesium isotope ratios. Earth Planet. Sci. Lett. 250, 241–253.

Tucker, M.E., 1991. Sedimentary Petrology: An Introduction to the Origin of Sedimentary Rocks. Blackwell Scientific Publications, Oxford.

Varol, B., Araz, H., Karadenizli, L., Kazanci, N., Seyitoglu, G., Sen, S., 2002. Sedimentology of the Miocene evaporitic succession in the North of Çankırı-Çorum Basin, central Anatolia, Turkey. Carbonate Evaporite 17, 197–209.

Veizer, J., Ala, D., Azmy, K., Bruckschen, P., Buhl, D., Bruhn, F., Strauss, H., 1999. $^{87}Sr/^{86}Sr$, $\delta^{13}C$ and $\delta^{18}O$ evolution of Phanerozoic seawater. Chem. Geol. 161, 59–88.

Vovnyuk, S.V., Czapowski, G., 2007. Generation of primary sylvite: the fluid inclusion data from the Upper Permian (Zechstein) evaporites. SW Poland: Geol. Soc. London, Special Publ. 285, 275–284.

Warren, J.K., 2016. Evaporites, A Geological Compendium. Springer, Switzerland.

Whitley, S., Gertisser, R., Halama, R., Preece, K., Troll, V.R., Deegan, F.M., 2019. Crustal CO_2 contribution to subduction zone degassing recorded through calc-silicate xenoliths in arc lavas. Science Report 9, 8803. https://doi.org/10.1038/s41598-019-44929-2.

Wombacher, F., Eisenhauer, A., Heuser, A., Weyer, S., 2009. Separation of Mg, Ca and Fe from geological reference materials for stable isotope ratio analyses by MC-ICP-MS and double-spike TIMS. J. Anal. At. Spectrom. 24, 627–636. https://doi.org/10.1039/b820154d.

Yavuz, N., Çulha, G., Demirer, Ş.S., Utescher, T., Aydın, A., 2017. Pollen, ostracod and stable isotope records of palaeoenvironment and climate: Upper Miocene and Pliocene of the Çankırı Basin (Central Anatolia, Turkey). Palaeogeography, Palaeoclimatol. Palaeoecol. 467, 149–165. https://doi.org/10.1016/j.palaeo.2016.04.023.